Theory and numerical modeling of electrical self-potential signatures of unsaturated flow in melting snow

Theory and numerical modeling of electrical self-potential signatures of unsaturated flow in melting snow

B. Kulessa,[1] D. Chandler,[2] A. Revil,[3,4] and R. Essery[5]

Received 25 February 2012; revised 11 June 2012; accepted 26 June 2012; published 8 September 2012.

[1] We have developed a new theory and numerical model of electrical self-potential (SP) signals associated with unsaturated flow in melting snow. The model is applicable to continuous natural melt as well as transient flow phenomena such as meltwater pulses and is tested using laboratory column experiments. SP signals fundamentally depend on the temporal evolution of snow porosity and meltwater flux, electrical conductivity (EC), and pH. We infer a reversal of the sign of the zeta potential (a fundamental electrical property of grain surfaces in porous media) consistent with well-known elution sequences of ions that cause progressive increases and decreases in meltwater pH and EC, respectively. Injection of fully melted snow samples, containing the entire natural range of ions, into melting snow columns caused additional temporary reversals of the sign of the zeta potential. Widely used empirical relationships between effective saturation, meltwater fraction, EC, and pH, as well as snow porosity, grain size, and permeability, are found to be robust for modeling purposes. Thus nonintrusive SP measurements can serve as proxies for snow meltwater fluxes and the temporal evolution of fundamental snow textural, hydraulic, or water quality parameters. Adaptation of automated multisensor SP acquisition technology from other environmental applications thus promises to bridge the widely acknowledged gap in spatial scales between satellite remote sensing and point measurements of snow properties. SP measurements and modeling may therefore contribute to solving a wide range of problems related to the assessment of water resource availability, avalanche or flood risk, or the amplification of climatic forcing of ice shelf, ice sheet, or glacier dynamics.

Citation: Kulessa, B., D. Chandler, A. Revil, and R. Essery (2012), Theory and numerical modeling of electrical self-potential signatures of unsaturated flow in melting snow, *Water Resour. Res.*, *48*, W09511, doi:10.1029/2012WR012048.

1. Introduction

[2] Snow is a complex natural material that undergoes metamorphosis as it ages, progressively altering its fundamental physical properties such as density, porosity, permeability, and grain size. Despite such inherent complexity, snow can be grouped into a finite number of well-recognized classes, as summarized in the *International Classification of Seasonal Snow on the Ground* [*Fierz et al.*, 2009], and snowpacks forming in different climates are expected to have distinctive structures [*Sturm et al.*, 1995]. There has been much recent progress in our understanding of fundamental snow hydrological properties and processes, owing particularly to measurements within well-defined, though typically small ($\sim$1 m^2), snow pits or lysimeters, allowing high-resolution tracking of evolving wetting fronts and quantification of rates of water percolation [*Staehli et al.*, 2004; *Campbell et al.*, 2006; *DeWalle and Rango*, 2008]. It remains challenging, however, to evaluate and calibrate fundamental snow hydrological properties, such as the Darcy velocity characterizing meltwater flux, at spatial scales that bridge the gap between such snow pit measurements and typical footprints of a few hundred meters achieved by satellite-based passive microwave sensing of snow hydrological and textural properties [*Domine et al.*, 2008; *Nolin*, 2010]. Our ability to quantify and assimilate spatially and temporally evolving hydrological properties and processes in snow models thus remains disproportionally poor compared with its anticipated significance in a range of applied snow hydrological problems [*Richter-Menge et al.*, 1991; *Williams et al.*, 1999]. These include, for instance, hydrological forecasting of snowmelt runoff that feeds rivers in many parts of the world [*Caine*, 1992; *Arnold et al.*, 1998; *Campbell et al.*, 2006], and the role of snowmelt in land-surface biogeochemical and geomorphological processes [*Caine*, 1995; *Williams et al.*, 2009]. Snowmelt is enhanced in a warming climate, amplifying of the dynamic response of the Antarctic and Greenland Ice Sheets or mountain glaciers to climatic forcing [*Fountain and Walder*, 1998; *Scambos et al.*, 2000; *Zwally et al.*, 2002], and mediating wet snow instabilities

[1]College of Science, Swansea University, Swansea, UK.
[2]Bristol Glaciology Centre, Bristol University, Bristol, UK.
[3]Department of Geophysics, Colorado School of Mines, Golden, Colorado, USA.
[4]ISTerre, UMR 5275, Université de Savoie, CNRS, Le Bourget du Lac, France.
[5]School of Geosciences, University of Edinburgh, Edinburgh, UK.

Corresponding author: B. Kulessa, College of Science, Swansea University, Singleton Park, Swansea SA2 8PP, UK. (b.kulessa@swansea.ac.uk)

0043-1397/12/2012WR012048

[*Mitterer et al.*, 2011]. The presence of liquid water strongly influences the electromagnetic properties of snow at microwave frequencies, and thus the interpretation of microwave remote sensing data [*Nolin*, 2010]. Melt and refreezing are important components of the energy balance of snowpacks, as parameterized in contemporary climate models [*Cline*, 1997; *Essery et al.*, 1999]. Many current snow models simply neglect water retention, which can however be expected to be significant in common snow hydrological settings [*Yamaguchi et al.*, 2010]. Such models unduly allow any meltwater to drain instantaneously from snow [*Essery et al.*, 1999], while others drain any water in excess of an irreducible saturation [*Dutra et al.*, 2010]. Other pertinent models [*Jordan*, 1991; *Dai and Zeng*, 1997; *Albert and Krajeski*, 1998; *Gustafsson et al.*, 2004] represent gravitational drainage at rates limited by the permeability of the snowpack [*Colbeck*, 1972]. A well-known deficiency of such models is the neglect of capillary effects, and they are found to perform better once the snow is fully saturated [*Cline*, 1997; *Gustafsson et al.*, 2004; *Jordan et al.*, 2008]. Other well-known deficiencies caused by the unavailability of suitable in situ hydrological data include a disregard of preferential vertical and horizontal flow paths [*Gustafsson et al.*, 2004; *Williams et al.*, 2010, and references therein]. Future progress in monitoring and quantifying snow hydrological processes thus depends on the development of new, preferably nonintrusive and nondestructive, techniques capable of estimating 2-D or 3-D water fluxes at spatial scales intermediate between snow pits and satellite footprints, as well as of the evolving physical and chemical properties of snow and snowmelt.

[3] Encouraged by recent work in several other environmental disciplines, we propose here fundamental developments of the electrical self-potential (SP) geophysical method for this purpose. Such work has ascertained the unique ability of the SP method in delineating, monitoring, and quantifying the flow of subsurface water in groundwater aquifers and unsaturated media [e.g., *Revil et al.*, 2006, and references therein], and indeed in a variety of cold regions applications [e.g., *French et al.*, 2006; *Kulessa*, 2007, and references therein]. This ability is based on the fact that pore waters generally have an excess of electrical charges due to the existence of an electrical double layer at the interface between the solid matrix (in the present case, the snow grains) and the pore water. The advective drag of this excess of electrical charge is responsible for a streaming current, whose divergence generates a quasistatic electric field known as the streaming potential [*Sill*, 1983; *Revil et al.*, 2003]. More recently, the streaming potential theory was extended for unsaturated conditions [*Linde et al.*, 2007; *Revil et al.*, 2007; *Jougnot et al.*, 2012]. It is well known that thermal gradients as well as gradients in the chemical potential of charge carriers (ions and electrons) can also generate SP signals [e.g., *Kulessa et al.*, 2003a; *Revil and Linde*, 2006; *Revil et al.*, 2010; *Doherty et al.*, 2010, and references therein]. As justified a posteriori in section 6.1, we have no reasons to expect strong thermal or chemical gradients to be generated in any of the laboratory experiments presented herein. We consider them to be negligible for the purpose of this study, but discuss the potential broader implications of their presence in field applications in sections 6 and 7.

[4] Following the pioneering work of *Sill* [1983], the SP theory for the semicoupled hydroelectric problem, neglecting electro-osmotic effects due to fluid flow forced by electrical current flow in the subsurface, is now well established for porous media with a skeleton composed of minerals (silica, aluminosilicates, and carbonates) that is saturated by water. In contrast, SP signals in snow are poorly understood and there is no fundamental theory to model the generation of streaming potentials in variably saturated snow. The principal goal of our work is therefore to develop such a theory and an associated numerical model for practical application to a wide range of snow hydrological problems. The new semicoupled hydroelectric model is tested using SP and snow hydrological, textural, and water-quality data collected using snow column experiments in the laboratory.

2. Theory and Model Description

2.1. Unsaturated Meltwater Flow in Snow

[5] For unsaturated conditions, the flow of meltwaters in a snowpack's pore space can be modeled by combining the Richards equation [*Richards*, 1931] with the van Genuchten-Mualem model, which parameterizes the effect of variable saturation of the liquid water phase upon the permeability and the capillary pressure [*van Genuchten* 1980; *Mualem* 1986; *Yamaguchi et al.*, 2010]. The Richards equation is given by

$$[C_e + S_e S]\frac{\partial H}{\partial t} + \nabla \cdot [-K\nabla(H+z)] = 0, \tag{1}$$

where t is time (in s), z is the elevation above a datum (in m), H is the total hydraulic head (in m), S is the storage coefficient (in m^{-1}), S_e is the effective saturation (dimensionless), K is the unsaturated hydraulic conductivity (in m s^{-1}), and C_e denotes the specific moisture capacity (in m^{-1}) defined by $C_e = \partial\theta/\partial H$. θ is the water content (dimensionless) defined by $\theta = S_w\phi$, where S_w is the relative saturation of the water phase (dimensionless) and ϕ represents the connected porosity of the material (dimensionless). The two saturations S_e and S_w are related to each other through the irreducible water saturation (S_w^{ir}) by

$$S_e = \frac{S_w - S_w^{ir}}{1 - S_w^{ir}}, \tag{2}$$

where S_w^{ir} denotes the residual saturation in a snowpack that is allowed to drain naturally by gravity. In the case of snow, it is often assumed that $S_w^{ir} \approx 0.03$, although S_w^{ir} is "one of the least well-understood parameters in snow physics" [*Albert and Krajeski*, 1998]. The unsaturated hydraulic conductivity, K, is related to the relative permeability, k_r, and the hydraulic conductivity at saturation, K_s, by $K = k_r K_s$. Following the van Genuchten-Mualem model, snow is saturated when the meltwater pressure reaches the atmospheric pressure ($H = 0$ at the water table, and H is negative in unsaturated conditions). In the van Genuchten-Mualem model, the effective saturation, S_e, the specific moisture capacity, C_e, the relative permeability, k_r, and the water content, θ, are given by

$$S_e = \begin{cases} \left[1 + |aH|^N\right]^{-M}, & H < 0 \\ 1, & H \geq 0 \end{cases} \tag{3}$$

$$C_e = \begin{cases} \frac{aM}{1-M}(\phi - \theta_r) S_e^{M-1}\left(1 - S_e^{M-1}\right)^M, H < 0 \\ 0, H \geq 0 \end{cases} \quad (4)$$

$$k_r = \begin{cases} S_e^L \left[1 - \left(1 - S_e^{\frac{1}{M}}\right)^M\right]^2, H < 0 \\ 1, H \geq 0 \end{cases} \quad (5)$$

$$\theta = \begin{cases} \theta_r + S_e(\phi - \theta_r), H < 0 \\ \phi, H \geq 0 \end{cases}. \quad (6)$$

The variable θ_r represents the residual water content ($\theta_r = S_w^r \phi$), and a, N, $M = (1 - N^{-1})$ and L are parameters that characterize the porous material [*Mualem*, 1978; *van Genuchten*, 1980]. The hydraulic conductivity at saturation, K_s, is defined as a function of the permeability, k, by $K_s = k\ \rho\ g\ \eta^{-1}$, where ρ and η are the meltwater density (in kg m^{-3}) and the dynamic viscosity (in Pa s), respectively, and g is acceleration of gravity (in m s^{-2}). Equation (5) is often approximated by $k_r = S_e^n$, where n is the effective saturation exponent [*Brooks and Corey*, 1964]. In the absence of direct evidence we follow *Albert and Krajeski* [1998] in using this relationship with $n \approx 3.3$.

2.2. Self-Potential Signals in Unsaturated Conditions

[6] The generation of an electrical field measured by the SP method is related to the existence of a source current density in the conductive porous medium. The total electrical current density **j** is given by an extended Ohm's law [*Sill*, 1983],

$$\mathbf{j} = \sigma \mathbf{E} + \mathbf{j}_S, \quad (7)$$

where **E** is the electrical field (in V m^{-1}) $\mathbf{E} = -\nabla\psi$, ψ is the electrical potential (in V), σ is the bulk electrical conductivity of the porous material (in S m^{-1}), and $\mathbf{j}_S$ is the source current density (in A m^{-2}). If the surface conductivity along the solid / pore water interface is neglected, the bulk electrical conductivity of the porous material, σ, is determined by

$$\sigma = \frac{1}{F} S_w^n \sigma_w \quad (8)$$

where F is the (intrinsic) formation factor and σ_w denotes the electrical conductivity of the pore water (abbreviated by EC hereinafter and expressed in S m^{-1}). Note that if S_w goes to zero (dry snow), the bulk conductivity would tend toward zero. To avoid this problem in the numerical computations, we keep the minimum water content in equation (8) equal to the irreducible water content (equation (2)).

[7] In the low-frequency limit of the Maxwell's equations, and without external injection or retrieval of charges, the continuity equation for the charge is given as [*Sill*, 1983]

$$\nabla \cdot \mathbf{j} = 0. \quad (9)$$

In this low-frequency limit, we consider that there is no storage of electrical charges in the porous material. In our case we can assume that the streaming current is the only contribution to the current density. The source current density is related to the relative saturation (S_w) and to the excess of charge, $\bar{Q}_V$ (in C m^{-3}), existing in the pore water by [*Revil et al.*, 2007]

$$\mathbf{j}_S = \frac{\bar{Q}_V}{S_w}\mathbf{u}, \quad (10)$$

where $\mathbf{u} = Q\ A^{-1}$ is the Darcy velocity (in m s^{-1}), Q is discharge (m^3 s^{-1}) and A is cross-sectional area (m^2). *Revil et al.* [2007] derived equation (10) using a volumetric averaging approach of the local Nernst-Planck equation. The excess of charge, $\bar{Q}_v$, represents the effective flux-averaged charge per unit pore volume that can be dragged by the flow of the pore water at saturation. The excess charge density, $\bar{Q}_v$, can be obtained directly from the permeability [*Jardani et al.*, 2007] at constant pH (typically 5 to 8) and salinity and pore water composition. Unfortunately the permeability-excess charge density relationship cannot be used for snow since the pH, composition, and salinity of the pore waters are expected to change significantly during snowmelt experiments. Combining equations (7) and (9), the SP field ψ is the solution of the Poisson equation,

$$\nabla \cdot (\sigma \nabla \psi) = \nabla \cdot \mathbf{j}_S. \quad (11)$$

The magnitude of SP signals is usually described by the streaming potential coupling coefficient (C_s) expressed in V m^{-1}. At saturation of the water phase C_s is defined by,

$$C_S = \left(\frac{\partial \psi}{\partial H}\right)_{j=0} = \frac{\bar{Q}_V\, k \rho_w g}{\eta \sigma}, \quad (12)$$

where the subscript s means "at saturation."

2.3. Hydraulic, Textural, and Chemical Properties of Snow

[8] Snow undergoes metamorphosis as it ages or is subject to the wetting of its pore space [*Brun*, 1989], causing progressive changes in its density, grain diameter and grain volume, as well as in its connected porosity and permeability as the surface-to-volume ratio of the snow grains evolves over time [*Jordan et al.*, 1999; *Domine et al.*, 2008]. Snowpacks are also subject to the preferential elution of ions in the early stages of melting, which follows well-known sequences and causes progressive and deterministic alterations of the EC and pH of the meltwaters in its pore space [e.g., *Brimblecombe et al.*, 1986; *Schöndorf and Herrmann*, 1987; *Cragin et al.*, 1993, 1996; *Davis et al.*, 1995; *Herrmann and Kranz*, 1995; *Harrington et al.*, 1996]. Variability in these snow properties can therefore lead to diagnostic changes in measured SP signals, and must therefore be parameterized in our numerical model. We introduce empirical descriptions of temporal changes in each of these properties in turn.

[9] Temporal changes in a metamorphosing snow sample's permeability are commonly [*Colbeck and Anderson*, 1982] estimated using *Shimizu*'s [1970] empirical formula,

$$k = 0.077 d^2 e^{-0.0078\rho_s}, \quad (13)$$

where ρ_s is snow density (in kg m^{-3}) and d is the mean diameter of the snow grains (in m). Equation (13) was derived from a fit to laboratory data collected with small

rounded grains and a starting grain diameter of ~0.33 mm [*Shimizu*, 1970]. However, *Jordan et al.* [1999] ascertained experimentally that *Shimizu*'s [1970] empirical formula does in fact apply to a much larger range of grain diameters expected to be encountered in practice (less than 0.5 mm to greater than 2 mm). We can therefore expect equation (13) to be robust for our modeling purposes. As the snow in the column becomes partially saturated, the snow grains undergo wet snow metamorphism, as characterized by an increase in grain diameter (d) and grain volume (v, in m^3), where

$$v(t) = \frac{4}{3}\pi\left(\frac{d}{2}\right)^3. \quad (14)$$

Brun [1989] found empirically that the increase of grain volume over time, $v(t)$, within a snow sample undergoing wet snow metamorphism, can be described by

$$v(t) = v(0) + (v_0 + v_1\theta)t, \quad (15)$$

where $v_0 = 1.28 \times 10^{-8}$ mm^3 s^{-1} and $v_1 = 4.22 \times 10^{-4}$ mm^3 s^{-1} are empirical constants. *Brun* [1989] obtained this relationship using a custom-built device to warm the snow samples, coupled with a dielectric system for the measurement of liquid water contents and a picture analyzer for the estimation of grain size. The mobility of liquid water at different states of saturation is a major constraint on grain growth.

[10] As demonstrated by several previous laboratory and field studies, some anions (specifically SO_4^- typically followed by NO_3^- and Cl^-) are commonly eluted first during the early stages of snowmelt [e.g., *Brimblecombe et al.*, 1986; *Schöndorf and Herrmann*, 1987; *Cragin et al.*, 1993, 1996; *Davis et al.*, 1995; *Herrmann and Kranz*, 1995; *Harrington et al.*, 1996]. Initial distributions of impurities in snowpacks and ion exclusion during snow crystal growth are key factors controlling specific elution sequences [*Davis et al.*, 1995; *Cragin et al.*, 1996]. An important consequence of the preferential elution of ions for our study is that meltwater pH commonly increases and EC decreases with increasing melt fractions. The experimental data of *Schöndorf and Herrmann* [1987], *Davis et al.* [1995] and *Herrmann and Kranz* [1995] reveal consistently that melt EC can be approximated empirically as an exponential function of the fractional melt, m_f (dimensionless) such that

$$\sigma_w = \sigma_0 e^{m_f m_0^{-1}}, \quad (16)$$

where σ_0 is melt EC at the start of the experiment (in S m^{-1}) and m_0 (dimensionless) is a constant that controls the rate of EC decrease over time, taking into account any effects of temperature upon EC. Since the experimental data of *Schöndorf and Herrmann* [1987, Figure 2] and *Davis et al.* [1995, Figure 2] consistently confirm that $m_0 \approx 0.08$, we adopt this value in our model. Measured EC (σ_{mean}) of the completely melted sample is equivalent to the mean value of σ_w between $m_f = 0$ and $m_f = 1$. Substituting $\sigma_w = \sigma_{mean}$ and successively inserting $m_f = 0$ and $m_f = 1$ into equation (16) allows the starting melt EC, σ_0, to be calculated using

$$\sigma_0 = \sigma_{mean}\left(m_0\left(1 - e^{-m_0^{-1}}\right)\right)^{-1}. \quad (17)$$

The snow samples of *Schöndorf and Herrmann* [1987], *Davis et al.* [1995] and *Herrmann and Kranz* [1995] were collected in different areas of the northern hemisphere (Fichtelgebirge (northeast Bavaria, Germany), Mammoth Mountain (California, USA), Campus of University Bayreuth (Germany), respectively) and had dissimilar compositions of the major ions. These authors' experiments were conducted over the entire range of melt fractions, $0 \le m_f \le 1$. We can therefore expect the exponential relationship between EC and melt fraction expressed in equations (16) and (17), and the choice of $m_0 = 0.08$, to be robust for our modeling purposes. Notwithstanding, we discuss the effects of potential variability in this relationship and in the parameter m_0 on our model results below.

2.4. Electrical Double Layer at the Ice-Water Interface

[11] The existence of a macroscopic electrical field associated with the flow of the pore water (i.e., the streaming potential) is related to the existence of a microscopic disturbance in the electrical properties of the pore water–solid interface called the electrical double layer. The existence of such an electrical double layer is well established, and models exist to compute its properties for silica [*Wang and Revil*, 2010] and clay minerals [*Leroy and Revil*, 2009]. In contrast, the electrochemical properties of the interface between natural snow or ice grains and liquid meltwaters contained within their pore spaces are poorly known. *Drzymala et al.* [1999] provided experimental data revealing the effect of the pH and the ionic strength of sodium chloride solutions upon the zeta potential of D_2O ice (made of heavy water). *Kallay et al.* [2003] provided the first double-layer model for the ice-water interface, which is conceptually similar to the type of model used for the silica water interface [e.g., *Leroy et al.*, 2008; *Wang and Revil*, 2010, and references therein]. A key difference arises in that the ice surface can attract anions, so that the position of the isoelectric point (or point of zero charge, for which the zeta potential is zero) within the pH spectrum is very sensitive to the concentrations of anions like Cl^-. Existing experimental data for H_2O and D_2O ice-water interfaces (Figure 1) indicate that the magnitude of the zeta potential decreases with acidic pH and that the isoelectric point can be expected to lie within the acidic region of the pH spectrum.

[12] Since the zeta potential (ζ) is a sensitive function of EC and pH [*Revil et al.*, 1999a, 1999b], it can be expected to vary considerably as a result of the preferential elution of ions from melting snow. Thus, we can assume that the combined dependency of ζ on EC (σ_w), meltwater pH (pH_w) and the meltwater pH at the point of zero charge (pH_w (pzc)) can be expressed as

$$\zeta(\sigma_w, pH) = [\alpha + \beta \log_{10}\sigma_w]\left(\sin\frac{\pi}{12}[pH_w - pH_w(pzc)]\right), \quad (18)$$

where α and β depend of the chemical composition of the pore fluid and can be determined empirically [*Revil et al.*, 1999b]. In accordance with previous laboratory work (Figure 1) and absence of suitable measurements in our own experiments, we adopt a point of zero charge ($pH_w(pzc)$) of 3.6 in our modeling experiments, and discuss the effects of potential variability in $pH_w(pzc)$ in section 6.4. We assume that meltwater pH, pH_w, has third-order polynomial dependency on meltwater fraction, as determined from a best fit

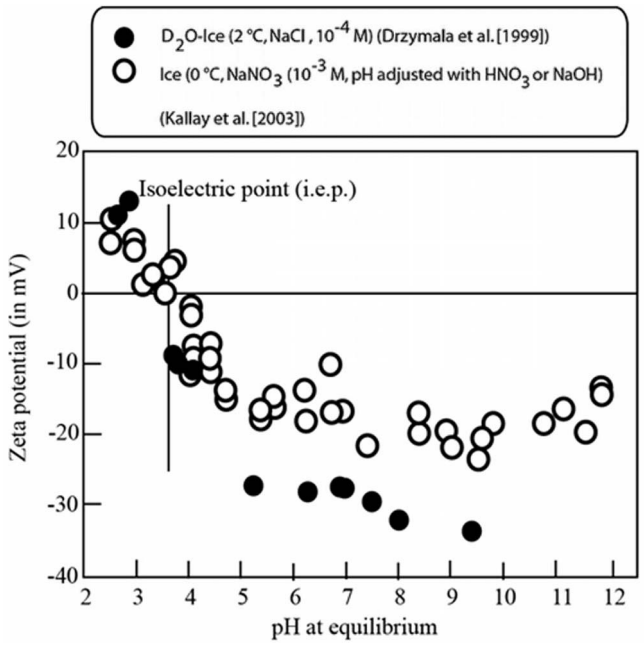

Figure 1. Zeta potential versus pH at two different salinities of sodium chloride solutions for H_2O ice and ice made of heavy water (D_2O) [*Kallay et al.*, 2003].

of the data presented by *Schöndorf and Herrmann* [1987] ($R^2 > 0.99$; see Figure 2), yielding:

$$pH_w = 5.03m_f^3 - 11.26m_f^2 + 8.33m_f + 3.25. \quad (19)$$

We assume that the fully melted snow samples have a pH of ≈6, representing the average (pH_{mean}) of the fully melted snow samples reported by *Darmody et al.* [2000] for the Kärgevagge region adjacent to the Abisko research station. The pH at the start of the experiment (pH_0) can then be calculated from $pH_0 = pH_{mean} - 1.67$, obtained by simple integration of the third-order polynomial fit reported in Figure 2 and equation (19).

3. Materials and Methods

[13] To test our new numerical model of SP signals generated by unsaturated water flow through melting snowpacks, we conducted a total of four repeat column experiments, classified as either a "natural melt experiment" or an "injection experiment." We used a wet laboratory in the Abisko Research Station, Arctic Sweden, in March 2007, which has a long record of snow depth measurements and research [*Kohler et al.*, 2006]. In the natural melt experiments we monitored the temporal evolution of the measured SP signals while the snow melted within our column (Figure 3) at a laboratory air temperature of ~21.5 ± 0.5°C (Table 1). The injection experiments adopted the same approach, except that fully melted snow samples were periodically injected into the melting snow column. Thus, both types of experiments effectively simulated snowpacks subject to intense melting due to rapid atmospheric temperature increases, consistent, e.g., with snow fall during the night and accelerated warming during the day. The injection experiments additionally simulated the effects of meltwater pulses flushing through a given location within a melting snowpack. Here we present one natural melt and one injection experiment, selected because they represented the longest records, had the best signal-to-noise ratios and had the highest sample rates of discharge and snow column geometries.

[14] Our laboratory column consisted of a Perspex tube, 32 cm long with respective inner and outer diameters of 5.9 cm and 6.5 cm, that terminated in a 4.5 cm long funnel and had a nominal volume of 897 cm^3 (Figure 3). Non-polarizing $Pb/PbCl_2$ electrodes, 5 cm long with a diameter of 1 cm, were custom built by downsizing the field version developed by *Petiau* [2000]. All custom-built electrodes were tested in a tap water bath, and were found to be stable to within 2×10^{-3} V over a period of several days, and thus over a much longer time period than the duration of our experiments (typically 5–6 h). The reference electrode was secured at the top of the snow column and the 'measurement' electrode at the column's base (Figure 3). A saturated sponge was wrapped around the base of the electrodes, ensuring good electrical contact between the two electrodes and the shrinking snow column at all times (Figure 3). Since the snow column melted away from the sides of the Perspex tube during the course of the experiment, we were unable to increase the number of measurement points by installing further electrodes along this snow column.

[15] In both experiments, the Perspex tube was filled with snow by inserting it into and subsequently removing it from the top few decimeters of undisturbed, meter-deep snowpacks well away from the research station. Although care was taken to minimize artificial snow compaction as much as possible, it is within the nature of this packing process that some compaction will occur compared to the snow's in situ state. The snow had fallen on the days prior to the experiments, and had not previously been exposed to sustained melt events. The snow was collected immediately prior to commencement of the laboratory experiments. Initial snow properties after column packing and environmental conditions are summarized in Table 1.

[16] To characterize cross-sectional and volume shrinkage rates, we measured the top and bottom diameters, as well as the length of the snow column, every 20 min throughout the duration of the experiment. All SP measurements were made at a sample rate of one second using a Campbell Scientific CR10 data logger, as used previously for this purpose

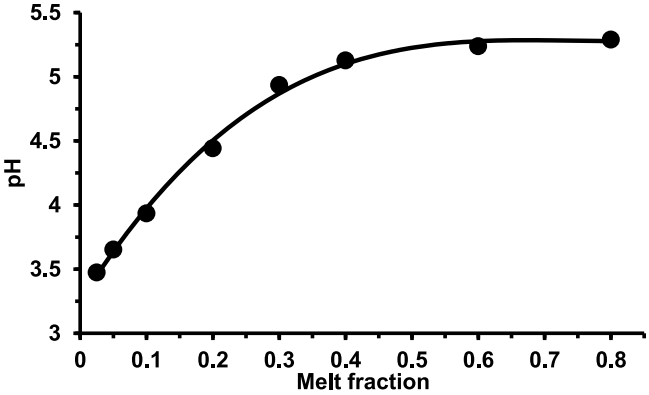

Figure 2. Third-order polynomial fit ($R^2 > 0.99$; see equation (19)) to the snowmelt data reported by *Schöndorf and Herrmann* [1987], reflecting increasing pH with melt fraction due to preferential elution of ions.

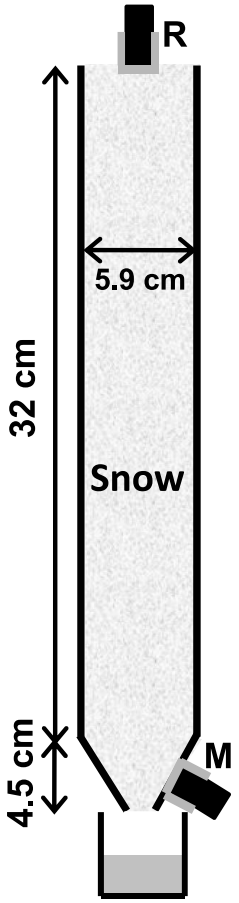

Figure 3. Schematic of our laboratory column setup. Saturated sponges (gray colors) were wrapped around the bases of the reference (R) and measurement (M) electrodes to ensure good contact. Meltwater discharge was collected in a beaker (as indicated) graduated with a sub-milliliter scale.

[*Kulessa et al.*, 2003a, 2003b]. These loggers have a very high input impedance of ~20 GΩ, which is several orders of magnitude larger than the impedance contrast between the reference and measurement electrodes (expected to be on the order of several MΩ) [*Kulessa et al.*, 2006; *Kulessa*, 2007]. Thus, the CR10 data loggers are well suited to measuring SP signals in highly resistive materials such as snow. Since available laboratory instrumentation was limited, we were unable to measure changes in either total or connected porosities, or other relevant hydrological or chemical properties (such as, e.g., EC or pH) during our experiments. In the injection experiment, 60 mL of snowmelt were injected at approximately 22.5, 83.5, 144.5, 202.5 and 263.3 min into the experiment. During each injection, the snowmelt was distributed across the upper face of the snow column over a period of a few seconds with a syringe. The injected snowmelt had a temperature close to 0°C and an EC of 0.0012 S m^{-1} (at 0°C; Table 1), and was taken from the same batch of snow that was used to fill the column during the injection experiment. In the natural melt experiment, no water was added to the snow column. Discharge from the base of the snow column was collected with a beaker, graduated with a sub-milliliter scale (Figure 3), every 10–30 s in the first few minutes following each injection, and every 60–300 s in between injections.

4. Experimental Results and Repeatability

[17] The overall temporal evolution of the measured SP signals was broadly similar for both the natural melt and the injection experiment (Figure 4a). Both SP signals were initially positive at 0.021 V (natural melt) and 0.014 V (injection), but rapidly decreased and changed sign after approximately one (natural melt) and five (injection) minutes into the experiment. The natural melt related SP signals are temporally variable, attaining minima of approximately −0.03 V and −0.04 V at ~25 min and ~140 min into the experiment that flank a temporary weakly positive peak (~+0.0025 V) at ~40 min (Figure 4a). From ~140 min onward the natural melt related SP signals rise steadily at a rate of ~+0.005 V min^{-1}, crossing zero at ~225 min and reaching a maximum of >+0.04 V at the end of the experiment. The injection-related SP signals attained minima of <−0.03 V between ~40 min and ~140 min (Figure 4a). At later times this signal rises at a rate comparable to that of the natural melt signal, and also crosses zero at approximately the same time. This baseline SP trend in the injection experiment is disrupted by the transient SP responses to the five injections, as labeled by numbers in Figure 4a. In each case the injection-related SP peaks are attained rapidly after injection and have positive peak values. Following an initial rapid period of decrease, these SP values typically remain higher than the pre-injection values for a few tens of minutes, eventually merging with the baseline SP signal. The first injection is a notable exception as the baseline signal is decreasing rapidly during the injection-related SP excursion. The temporary weakly positive SP peak at ~40 min, prominent in the natural melt SP signal, is not observed in the injection-related SP data (Figure 4a).

[18] Following the first meltwater breakthrough at ~50 min into the natural melt experiment, specific discharge, $Q\,A^{-1}$ (equal to Darcy velocity **u**, equation (10)), increases approximately linearly at a rate of ~4×10^{-5} m min^{-1} (Figure 4b). Following the first injection at ~22.5 min, the first meltwater breakthrough occurred at ~24.7 min in the injection experiment (Figure 4b). The baseline trend of specific discharge for the injection experiment, characterized by the specific discharge values between the five sequential injections, is broadly similar to the natural melt trend. The breakthrough curves for the five sequential injections readily reflect increasing peaks in specific discharge (Figure 4b). A close comparison of Figures 4a and 4b reveals that for each of

Table 1. Snow Densities and Porosities at the Start of the Natural Melt and Injection Experiments, Along With Meltwater ECs of the Fully Melted Snow Samples, as Well as Ambient Outside and Inside Laboratory Temperatures

Property	Natural Melt	Injection
Density (kg m^{-3})	482	526
Porosity	0.52	0.47
σ_{mean} (S m^{-1})	0.007	0.0012
$T_{outside}$ (°C)	−2	−1
T_{inside} (°C)	+21	+22

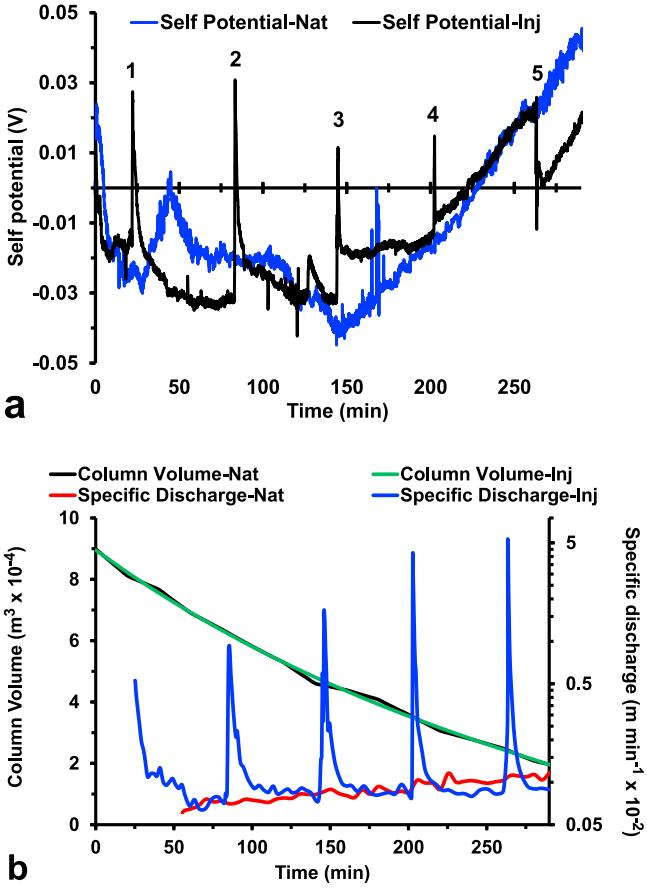

Figure 4. (a) Streaming potential data measured during the natural melt (Nat) and injection (Inj) experiments. The five sequential meltwater injections are labeled. (b) Changes in column volume and specific discharge over the course of these experiments.

the five injections, the SP peaks lead the discharge peaks. Specifically, the lags are ~2.5 min for the first injection, ~0.5 min for the second and third injection, and <0.5 min for the fourth and fifth injections. The decrease in column volume, calculated using equation (23), is remarkably similar for the natural melt and injection experiments (Figure 4b).

[19] It is encouraging that the inferred decreases in column volume are almost identical for the natural melt and injection experiments (Figure 4b), and that the overall temporal evolutions of the natural melt and injection-related SP signals were broadly similar (Figure 4a). Indeed, all of our four repeat column experiments were characterized by the same general temporal evolutions of SP signals and column volume. We can therefore conclude with some confidence that the data presented here were representative and repeatable.

5. Numerical Modeling

5.1. Solution to Governing Equations

[20] In the case of our laboratory column experiments, we assume that the electrical potential at the reference electrode at the top of the column is zero, and that there is no external injection or retrieval of electrical charge. At any given point in time, any melt is assumed to be uniformly distributed within the snow column. This is a distinct simplification of real flow systems, as discussed in detail in sections 6.2 and 7. The electrical streaming current generated by the downward movement of the snowmelt within the confines of the column is, thus, the only source of the current density $\mathbf{j}_s$. We assume insulating boundary conditions on all inner faces of our snow tube. The solution to equation (11), and thus the SP field ψ, is in this situation given by the classic Helmholtz-Smoluchowski theory, extended for unsaturated flow by the unsaturated streaming potential coupling coefficient $C_{unsat} \approx C_s S_w$ (V m^{-1}) [*Guichet et al.*, 2003; *Revil and Cerepi*, 2004]. Adapting *Guichet et al.* [2003, equation (8)], we can write

$$\psi_m - \psi_0 = -C_{unsat}(H_m - H_0) = -\frac{\varepsilon\xi}{\eta\sigma_w} S_w (H_m - H_0), \qquad (20)$$

where ψ_m and H_m are respectively the electrical and hydraulic potentials at the measurement electrode, and $\psi_0 = H_0 = 0$ are the corresponding potentials at the reference electrode. Assuming that water at 0°C has a dielectric permittivity of $\varepsilon_r = 88$, the dielectric permittivity (F m^{-1}) of pore meltwater is $\varepsilon = \varepsilon_r \varepsilon_0 = 7.8 \times 10^{-9}$ F m^{-1}, where $\varepsilon_0 = 8.85 \times 10^{-12}$ F m^{-1} is the dielectric permittivity of vacuum. Since neither laboratory temperature nor those of the snow column or snowmelt are expected to change by more than 1°C over the course of our experiments (section 3), we can assume that any temperature-related changes in ε are negligible. A comparison of equations (12) and (20) reveals that, for our column experiment, the relationship between the excess of charge, $\bar{Q}_V$, and the zeta potential (ζ) is

$$\bar{Q}_V = \frac{\varepsilon\zeta}{kF} S_w. \qquad (21)$$

Equation (21) implies that as long as the permeability and the formation factor (and hence the connected porosity) are independent of the pH and the salinity of the pore waters, the pH and salinity dependence of the excess of charge are controlled by the pH and salinity dependence of the zeta potential.

[21] We are particularly interested in determining the relationship between the two measured quantities ψ_m (SP at the measurement electrode) and Q (discharge from the base of the column). Since we have also measured changes in mean snow column cross-sectional area (A), this is conveniently achieved by combining equations (8), (10), (20) and (21), yielding:

$$\psi_m = \frac{\varepsilon\zeta}{\sigma_w} \frac{S_w}{S_e^n} \frac{1}{kA} Q. \qquad (22)$$

Equation (22) can be used to model the streaming potential (ψ_m) for a given water flux Q.

[22] As explained in section 3, there are several temporally evolving parameters in our model that we were unfortunately unable to measure during the course of our experiments. However, we are able to use existing theory, empirical relationships or previous observations to place tight constraints on all of these parameters but two; those exceptions are initial grain volume ($v(0)$, equation (15)) and the temporal evolution of snow porosity (ϕ). As argued in

more detail in section 5.3, we can confidently restrict the uncertainty range of v_0 to the *fine* grain-size category (0.2–0.5 mm; see *Fierz et al.* [2009]). We can calculate the initial total porosities at the start of both the natural melt (ϕ_{ini} = 0.52) and injection (ϕ_{ini} = 0.47) experiments, and assume that the "effective total porosity" is equal to ϕ_{ini} $(1 - S_w^{ir})$ = 0.97 * ϕ_{ini} [*Colbeck*, 1972]. *Schwander et al.* [1993] reported measurements of the connected (termed 'open' in their work) and closed porosities in a variety of Polar snow and firn samples. They found that connected porosity was effectively equal to total porosity below snow densities of ~800 kg m^{-3}, which was the case throughout our laboratory experiments. We do not, however, have tight constraints on either the temporal evolution or the total porosity values at the end of the experiments. Consistent evidence for the temporal evolution of either the total or the connected porosities of melting snow has not yet been published in the literature accessible to us. We therefore make the two assumptions that [a] the inferred values of effective total porosity (i.e., 0.97 × ϕ_{ini}) at the start of the two experiments can serve as proxies for the corresponding connected porosities; and [b] that connected porosities evolve linearly during our 6 h long experiments between the starting values and a range of assumed final porosities that place uncertainty constraints on our model outputs. To avoid confusion we use the term 'snow porosity' or simply 'porosity' in the remainder of this manuscript. It is implicit in this usage that we are referring to the 'connected porosity' that governs permeability and discharge, both of which are key controls on the magnitude of the measured SP signals according to equation (22).

5.2. Model Implementation

[23] The mean snow saturation, S_w, was calculated using measurements of snow column dimensions and discharge, based on the assumption that the initial water content was zero. It was further assumed that changes in snow column volume were purely due to uniformly distributed melt. In the case of the injection experiment, it was assumed that any slug of water injected at the top of the column was equally distributed across the available cross-sectional area of the snow column during downward movement. Each experiment yielded a series of measurements at times $t_{(i)}$, $i = 1 \ldots N$. At each $t_{(i)}$ we have the following data: (1) $\Delta Q_{(i)}$ [m^3] is the melt discharge between $t_{(i-1)}$ and $t_{(i)}$; (2) $H_{c,(i)}$ [m] is the snow column height above the top of the funnel (Figure 3); (3) $d_{T,(i)}$ [m] is the snow column diameter at the top of the column; (4) $d_{B,(i)}$ [m] is the snow column diameter at the base of column (top of funnel); (5) $V_{inj,(i)}$ [m^3] is the volume of water injected between $t_{(i-1)}$ and $t_{(i)}$.

[24] The SP measurements were conducted at a much higher sampling rate (1 s) than those of discharge and column geometry. In both the natural melt and the injection experiments the temporal evolution of snow column geometry was measured every 20 min. In the case of the natural melt experiment discharge was measured every five minutes, while average discharge sampling rate in the injection experiment was ≈2.4 min. The latter rate was increased to a maximum of 15 s during the final (fifth) injection, but was decreased to a minimum of 5 min in between injections. For our modeling purposes it is most appropriate to seek to predict a streaming potential value for each discharge measurement. Since any such measurement represents an average over the time period during which the melt was collected in the graduated beaker (Figure 3), the SP data were subsampled by averaging over the same time period. The standard deviation of the SP data, recorded at much higher sampling rate within any such time period, thus indicates inherent modeling uncertainty. The column geometry measurements, recorded on a smaller timescale than the discharge measurements, were linearly interpolated to match the discharge sampling rate, as justified by the near-linear decreases in column volume (Figure 4b).

[25] From measuring the mass and volume of snow in the column we can readily calculate the total snow porosity, ϕ_{ini}, at the start of the experiment, taken as a proxy value for the initial connected porosity (section 5.1). Using the mass densities of pure ice (ρ_i = 917 kg m^{-3}) and pure water (ρ_w = 1000 kg m^{-3}), we can now estimate the column volume ($V_{C,(i)}$) as

$$V_{C,(i)} = \pi H_{c,(i)} \left[{}^1\!/_4 \left(d_{T,(i)} + d_{B,(i)} \right) \right]^2 + V_{f,(i),} \tag{23}$$

where funnel volume is $V_{f,(i)} = 1/3\pi(d_{B,(i)}/2)^2 h_f$ and funnel height is h_f = 0.045 m. The volume of meltwater ($\Delta V_{m,(i)}$) generated over the time interval t_{i-1} to t_i is

$$\Delta V_{m,(i)} = (\rho_i/\rho_w) \left[\left(1 - \phi_{(i-1)}\right) V_{C,(i-1)} - \left(1 - \phi_{(i)}\right) V_{C,(i)} \right]. \tag{24}$$

The total melt ($V_{m,(i)}$) and total discharge (Q_i) generated since the start of the experiment are then, respectively,

$$V_{m,(i)} = V_{m,(i-1)} + \Delta V_{m,(i)} \tag{25}$$

$$Q_{(i)} = Q_{(i-1)} + \Delta Q_{(i).} \tag{26}$$

Consideration of the overall water balance gives the total water storage ($V_{S,(i)}$) and mean saturation ($S_{w,(i)}$) in the column as:

$$V_{S,(i)} = V_{m,(i)} + V_{inj,(i)} - Q_{(i)} \tag{27}$$

$$S_{w,(i)} = V_{S,(i)} \left(V_{C,(i)} \phi_{(i)} \right)^{-1}. \tag{28}$$

In the case of the injection experiment, at any given time $t_{(i)}$ EC (σ_{mix}) and pH (pH$_{mix}$) are effective *mixed* values. These are integrated over those of the total volumes of natural melt and injected meltwaters moving within the column at that time. The mixed values were calculated as:

$$\sigma_{mix,(i)} = V_{m,\%,(i)} \sigma_{m,(i)} + V_{inj,\%,(i)} \sigma_{mean} \tag{29}$$

$$pH_{mix,(i)} = V_{m,\%,(i)} pH_{m,(i)} + V_{inj,\%,(i)} pH_{mean}, \tag{30}$$

where $V_{m,\%,(i)}$ and $V_{inj,\%,(i)}$ are the percentage volumes of natural melt and injected meltwaters stored within the column at time $t_{(i)}$, $\sigma_{m,(i)}$ and pH$_{m,(i)}$ are respectively the EC and pH of the melt at that time, and σ_{mean} = 0.0012 S m^{-1} and pH$_{mean}$ = 6. In calculating $V_{m,\%,(i)}$ and $V_{inj,\%,(i)}$ we must allow for the finite amount of time it takes for the injected meltwaters to reach the outlet at the base of the column. This was implemented by adopting the common formulation that the injected slug of water flows within the column

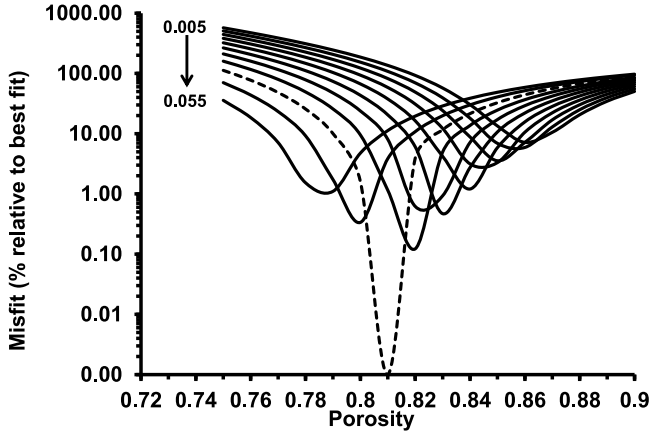

Figure 5. Sensitivity of the misfit between measured and modeled streaming potential data, relative to the best fit, in the natural melt experiment. Misfit is dependent upon unknown final porosity (ϕ_{fin}, abscissa) and unknown initial grain volume ($v(0)$, range of curves for 0.005–0.055 mm^3). Misfit is determined from the sum of squared residuals, as explained in section 5.2. The best fit occurs for $\phi_{fin} = 0.81$ and $v(0) = 0.015$, as indicated by the dashed line.

at a velocity ($vel_{inj,(i)}$) of

$$vel_{inj,(i)} = u_{(i)}\phi_{(i)}^{-1}, \tag{31}$$

where $u = Q\,A^{-1}$ is the magnitude of the Darcy velocity. Specifically, we assume that the time ($t_{delay,(j)}$, where j denotes the j^{th} injection) it takes for the leading edge of the injected slug to reach the base of the column during the j^{th} injection is $t_{delay,(j)} = (H_{c,(j)} + 1/3\ h_{f,(j)})/vel_{inj,(j),\max}$, where $vel_{inj,(j),\max}$ is the maximum velocity attained during the j^{th} injection. Thus, at that particular time ($t_{delay,(j)}$) the injected meltwaters is assumed to be equally distributed across the available pore space within the snow column, mixing uniformly with the amount of the melt stored within the column at that time according to the relative percentages $V_{m,\%,(i)}$ and $V_{inj,\%,(i)}$. Accordingly, at times $t_{(j)} > t_{delay,(j)}$ we can assume that the meltwaters discharged from the base of the column are also partitioned into melt and injected meltwaters according to these percentages. Within the time interval $0 < t_{(j)} < t_{delay,(j)}$, $V_{inj,\%,(i)}$ is proportionally decreased and $V_{m,\%,(i)}$ proportionally increased according to fractional column volume occupied by the injected slug as it propagates down column.

[26] We can now model the zeta potential ($\zeta_{mod,(i)}$) and streaming potential ($\psi_{mod,(i)}$) by, first, calculating the zeta potential ($\zeta_{\exp,(i)}$) expected from our streaming potential measurements ($\psi_{meas,(i)}$) following equation (22):

$$\zeta_{\exp,(i)} = \frac{\sigma_{w,(i)} S_{e,(i)}^{n} k_{(i)}}{\varepsilon S_{w,(i)} q_{(i)}}\psi_{meas,(i)}. \tag{32}$$

Second, using equation (18) we can then correct $\zeta_{\exp,(i)}$ for the effects of variable pH to obtain $\zeta_{crrct,(i)}$:

$$\zeta_{crrct,(i)} = \frac{\zeta_{\exp,(i)}}{\sin\frac{\pi}{12}\left(pH_{w,(i)} - pH_w(pzc)\right)} = \alpha + \beta\log_{10}\sigma_{w,(i)}. \tag{33}$$

Following equation (33) we can then estimate the empirical constants α and β by linear regression of $\zeta_{crrct,(i)}$ and $\log(\sigma_{w,(i)})$. This procedure effectively calibrates the zeta potential in terms of pH and EC. Significantly from a field application perspective, it is now possible to calculate the modeled zeta potential ($\zeta_{mod,(i)}$) directly from measured EC ($\sigma_{w,(i)}$) and $pH_{w,(i)}$ using equation (18). The time series of modeled streaming potential ($\psi_{mod,(i)}$) can subsequently be calculated using

$$\psi_{\mathrm{mod},(i)} = \frac{\varepsilon}{\sigma_{w,(i)}}\frac{S_{w,(i)}}{S_{e,(i)}^{n}}\frac{u_{(i)}}{k_{(i)}}\zeta_{\mathrm{mod},(i)}. \tag{34}$$

Model application involves manual adjustment of the two unknown parameters, final porosity (ϕ_{fin}) and initial grain volume ($v(0)$), until the misfit between measured and modeled streaming potentials is minimized in a linear least squares sense. The sum of the squared residuals serves as the measure of the goodness of fit, and in the natural melt experiment is normalized by the difference between the maximum and minimum value of the modeled zeta potential (ζ_{mod}) to honor previous laboratory measurements (Figure 1).

5.3. Modeling Results for Natural Melt Experiments

[27] As is readily appreciated from our sensitivity study summarized in Figure 5, the fit between measured and modeled streaming potentials was relatively poor outside the ranges of final snow porosities (ϕ_{fin}) of 0.75–0.9, and of 0.005–0.055 mm^3 for initial grain volume ($v(0)$). We have therefore restricted our natural melt and injection modeling experiments to these ranges of ϕ_{fin} and v_0, and discuss the implications in section 6.2. In accordance with equation (14), the range of values of v_0 (0.005–0.055 mm^3) spans the entire spread of the fine grain-size category (0.2–0.5 mm) [*Fierz et al.*, 2009]. Specifically, this range also includes $v_0 \approx$ 0.015–0.02 mm^3 as measured by both *Shimizu* [1970, Figure 10] and *Brun* [1989, Figure 5], whose empirical grain size–permeability (equation (13)) and grain-growth relationships (equation (15)) are parameterized in our numerical model. We found that the best fit between measured and modeled SP signals was obtained for $\phi_{fin} = 0.81$ and $v_0 = 0.015$ (Figure 5), and define our range of uncertainty as any combination of final porosities (where $0.75 \le \phi_{fin} \le 0.9$) and initial grain volumes (where 0.005 mm^3 $\le v(0) \le$ 0.055 mm^3) that deviated by 10% or less from this best fit.

[28] Within the 10% uncertainty range, modeled effective saturation increased nonlinearly from zero at the start of the experiment, to ~0.43 after 140 min (Figure 6a). Only minor fluctuations around this value are observed from this point until the end of the experiment at 300 min. Permeability was modeled to increase by more than two orders of magnitude from $2.7 \pm 0.5 \times 10^{-10}$ m^2 at the start of the experiment to $5.8 \pm 0.8 \times 10^{-8}$ m^2 after 300 min, and grain diameter to increase approximately linearly from 0.35 ± 0.04 mm to 1.66 ± 0.05 mm (Figure 6a). Over the same time period, and using the same 10% uncertainty range, modeled EC decreased exponentially by some five orders of magnitude from $\sim 8.75 \times 10^{-2}$ S m^{-1} (associated uncertainty $\ll$ 1%) to $5.93 \pm 0.39 \times 10^{-7}$ S m^{-1} (Figure 6b). Meltwater pH was modeled to increase rapidly from 4.3 to 6.3 over the first 100 min of the experiment, whence it remained approximately constant (Figure 6b). Within the 10% uncertainty range, the modeled sensitivity of all five parameters (i.e.,

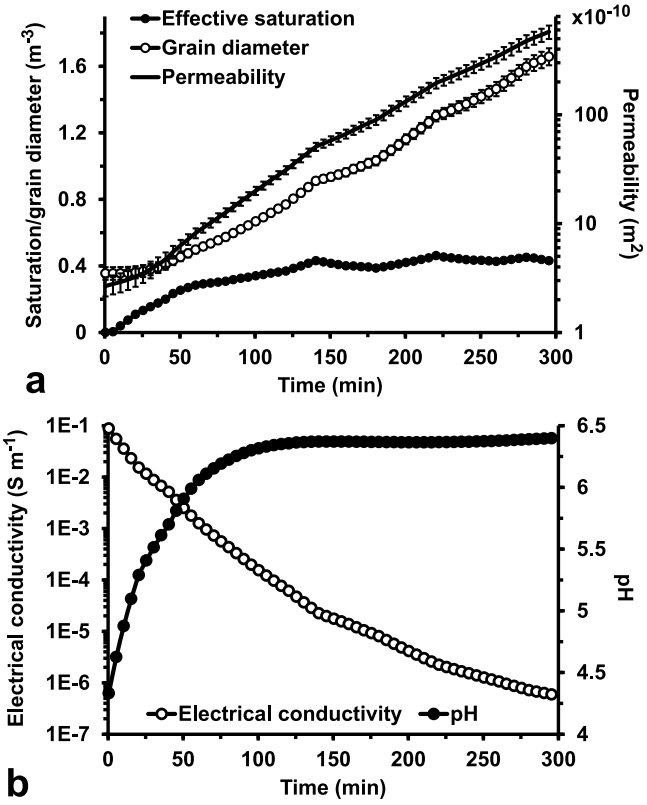

Figure 6. Model outputs for the natural melt experiment, using the best fit parameters of final porosity (ϕ = 0.81) and initial grain volume ($v(0)$ = 0.015 mm^3), and a 10% uncertainty range as explained in section 5.3. (a) Changes in three inferred snow properties. (b) Inferred changes in EC and pH due to preferential elution of ions. Note that permeability in Figure 6a and EC in Figure 6b are displayed using logarithmic scales. Calculated error bars for effective saturation in Figure 6a and both curves in Figure 6b are smaller than the size of the markers used.

effective saturation, permeability, grain diameter, EC and pH; see Figure 6), to variations in final porosity (ϕ_{fin}) and initial grain volume ($v(0)$) was small.

[29] Following the procedure described in section 5.2, and adopting the 10% uncertainty range, we have successively (i) calculated expected zeta potentials (ζ_{exp}; see Figure 7a) from equation (32) for the range of final porosities ($0.75 \leq \phi_{fin} \leq 0.9$) and initial grain volumes (0.005 mm^3 $\leq v(0) \leq$ 0.055 mm^3) considered, (ii) corrected ζ_{exp} for temporal changes in pH, yielding ζ_{crrct}, and (iii) plotted ζ_{crrct} against the decadal logarithm of the EC ($\log(\sigma_w)$) (Figure 7b). Since the first meltwater discharge occurred only at ~50 min into the experiment (Figure 4b), we are not able to model the measured SP data before that time. The expected zeta potential (ζ_{exp}) initially decreases from ~50 to 60 min into the experiment to reach a minimum of $-10.9 \pm 0.9 \times 10^{-2}$ V, whence it increases steadily except for the time period 105–145 min where it remains approximately constant or decreases slightly (Figure 7a). ζ_{exp} becomes positive at ~230 min into the experiment, and reaches a maximum of $+14.4 \pm 0.2 \times 10^{-2}$ V at ~285 min (Figure 7a). As expected from equation (33), we obtain a statistically significant linear relationship between ζ_{crrct} and $\log(\sigma_w)$ (Figure 7b), characterized by $\alpha = -4.4 \times 10^{-2}$ V and $\beta = 25.2 \times 10^{-2}$ V. Now that estimates of α and β are available, we can calculate the modeled zeta potential (ζ_{mod}; see Figure 7a) directly from inferred EC using equation (18), and subsequently the modeled streaming potential ($\nabla\phi_{mod}$) from ζ_{mod} using equation (34). Using a fixed point of zero charge (pH$_w$(pzc)) of 3.6 as introduced in section 2.4, ζ_{mod} increases steadily from -8.7×10^{-2} V to $+1.5 \times 10^{-2}$ V (red curve in Figure 7a). We obtain an excellent agreement between measured and modeled streaming potentials (Figure 8), characterized by uncertainty bounds that are remarkably small and thus document a weak sensitivity of modeled streaming potentials to the combined uncertainty in final porosity (ϕ_{fin}) and initial grain volume ($v(0)$) (Figure 8).

5.4. Modeling Results for Injection Experiment

[30] In the natural melt experiment we inferred that preferential elution of snowpack ions generated characteristic variations in meltwater EC and pH (Figure 6b). This caused the modeled zeta potential (ζ_{mod}) to increase from $-8.7 \times$

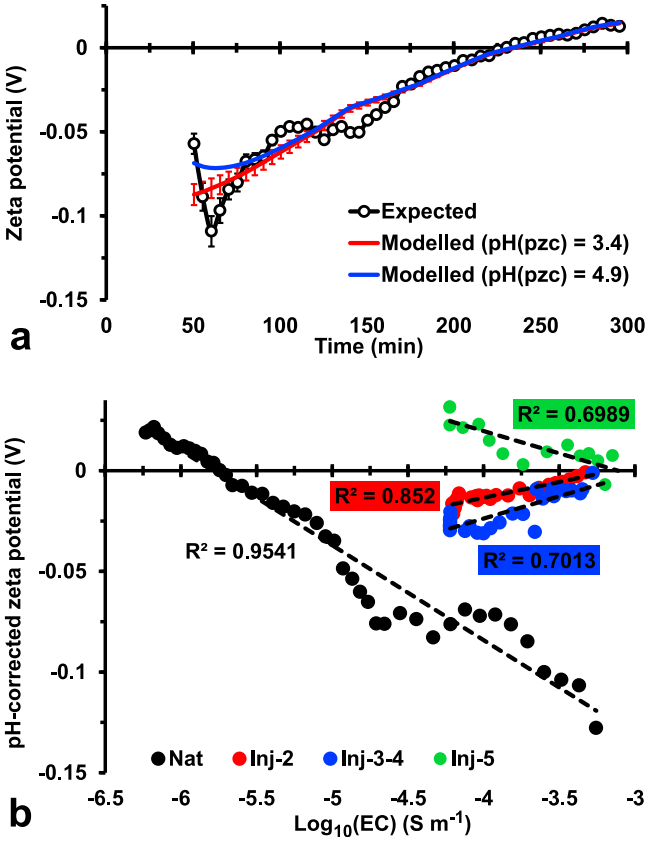

Figure 7. Model outputs for the natural melt and injection experiments using the same values of final porosity (ϕ = 0.81) and initial grain volume ($v(0)$ = 0.015 mm^3). (a) Time series of expected (ζ_{exp}) and modeled zeta potentials (ζ_{mod}) for the natural melt experiment, using two different values of the point of zero charge (pH(pzc)) and a 10% uncertainty range, as explained in section 5.3. (b) Scatterplots of zeta potential, corrected for pH (ζ_{crrct}), against the decadal logarithm of EC for the natural melt experiment (Nat) and for injections 2 (Inj-2), 3 and 4 (3–4), and 5 (Inj-5).

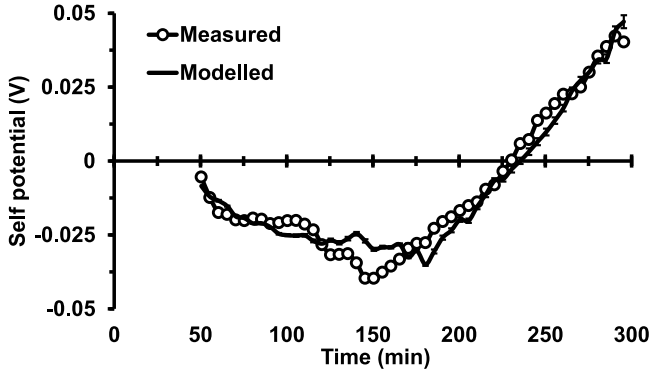

Figure 8. Time series of measured and modeled streaming potential data for the natural melt experiment, using the best fit parameters of final porosity (ϕ = 0.81) and initial grain volume ($v(0)$ = 0.015 mm^3), and a 10% uncertainty range as explained in section 5.3.

10^{-2} V to +1.5 $\times$ 10^{-2} V over the course of the 6 h experiment (Figure 7a), and was characterized by one set of values for α (-4.4×10^{-2} V) and β (25.2×10^{-2} V) that control the relationship between the corrected zeta potential (ζ_{crrct}) and meltwater EC (Figure 7b). Snow column shrinkage rates, and thus rates of meltwater production, were effectively identical for both the natural melt and injection experiments (Figure 4b), which typifies the encouraging repeatability of our experiments (section 4). We can therefore expect that the preferential elution of ions, and thus its diagnostic effect on meltwater EC and pH, progresses in a similar manner in the injection experiment as compared with the natural melt experiment. However, at hourly intervals over the course of the experiment (Figure 4), we injected fully melted snow samples into the column that contained the entire range of snowpack ions. Thus, the chemical composition of the pore waters will evolve in a more complex manner compared to the natural melt experiment. Since the values of α and β critically depend on the ionic composition of the pore waters [*Revil et al.*, 1999b], we cannot therefore expect that one single set of these values characterizes the relationship between EC and ζ_{crrct} in the injection experiment, as discussed further in section 6.4. Rather, we expect α and β to vary in a systematic manner over time, and therefore model our sequential injection experiments individually. We follow the procedure outlined in section 5.2 and applied earlier to the natural melt experiment. Since there is no reason to expect that the initial grain volume ($v(0)$) should be different in the injection experiment as compared with the natural melt experiment, we have for consistency kept v_0 constant at 0.015 mm^3, corresponding to the best fit value in the natural melt experiment (section 5.3). The best matches between measured and modeled streaming potential data for injections 2 to 5 were then obtained when final porosities (ϕ_{fin}) were equal to 0.81 $\pm$ 0.06. Allowing for the statistical variability, these values are similar as compared with each other and with the natural melt experiment (section 5.3). All of the modeling results included here were therefore obtained using ϕ_{fin} = 0.81 and v_0 = 0.015 mm^3.

[31] Effective saturation is modeled to have a baseline value of ~0.2 in between injections, transiently increasing to ~0.4 in response to snowmelt injections 2 to 5 (Figure 9a). Only at the start and end of the injection experiment is effective saturation less than 0.2. Permeability was modeled to increase by approximately one order of magnitude from 3.1 $\times$ 10^{-10} m^2 at the start of the experiment to 1.4 $\times$ 10^{-9} m^2 after 300 min, and grain diameter to increase steadily from 0.15 mm to 0.88 mm (Figure 9a). EC is modeled to decrease rapidly within the first half hour of the experiment, from ~15 $\times$ 10^{-3} S m^{-1} to less than 0.5 $\times$ 10^{-3} S m^{-1}, and pH to increase rapidly from 4.33 to greater than 6 (Figure 9b). During the remainder of the experiment, injection-related peak-to-peak EC variations of ~0.5–0.75 $\times$ 10^{-3} S m^{-1} are superimposed on a baseline EC of ~6 $\times$ 10^{-5} S m^{-1} (Figure 9b). Over the same time interval pH variations of opposite phase to the EC variations, and peak-to-peak amplitudes of between ~0.1 (earlier times) and ~0.3 (later times) are superimposed on a gradually increasing pH baseline trend (Figure 9b). Thus, the temporal evolution of meltwater pH is very similar for the natural melt (Figure 6b) and injection (Figure 9b) experiments, except for the brief pH excursions caused by the five sequential injections. In contrast, meltwater EC decreases much more rapidly over the first hour in the injection (Figure 9b) compared to the natural melt (Figure 6b) experiment, and baseline values at later times (>100 min) remain approximately one order of magnitude higher in the injection (~6 $\times$ 10^{-5} S m^{-1}; see Figure 9b) compared to the

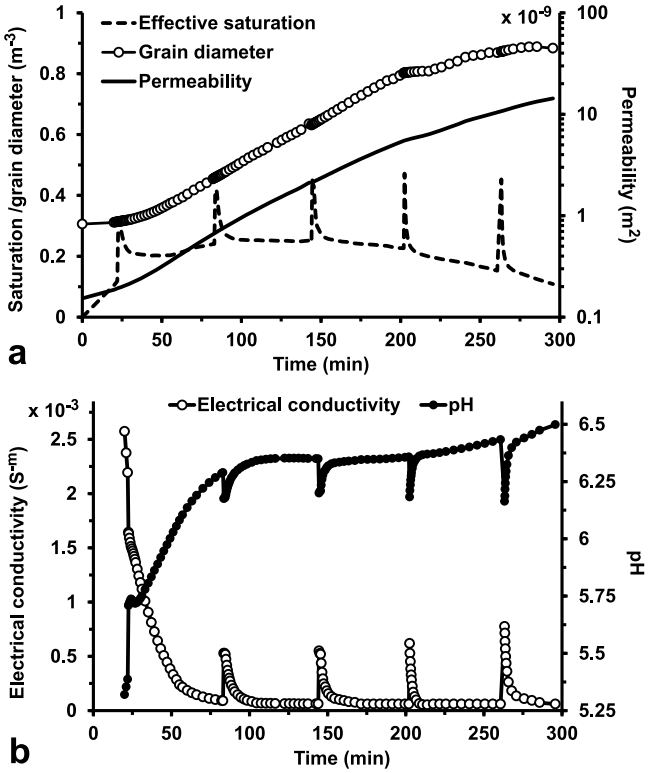

Figure 9. Model outputs for the injection experiment. (a) Changes in three inferred snow properties using, for consistency, the same final porosity (ϕ = 0.81) and initial grain volume ($v(0)$ = 0.015 mm^3) as in natural melt experiment. Note that permeability in Figure 9a is displayed using logarithmic scales. (b) Inferred changes in EC and pH using the same parameters.

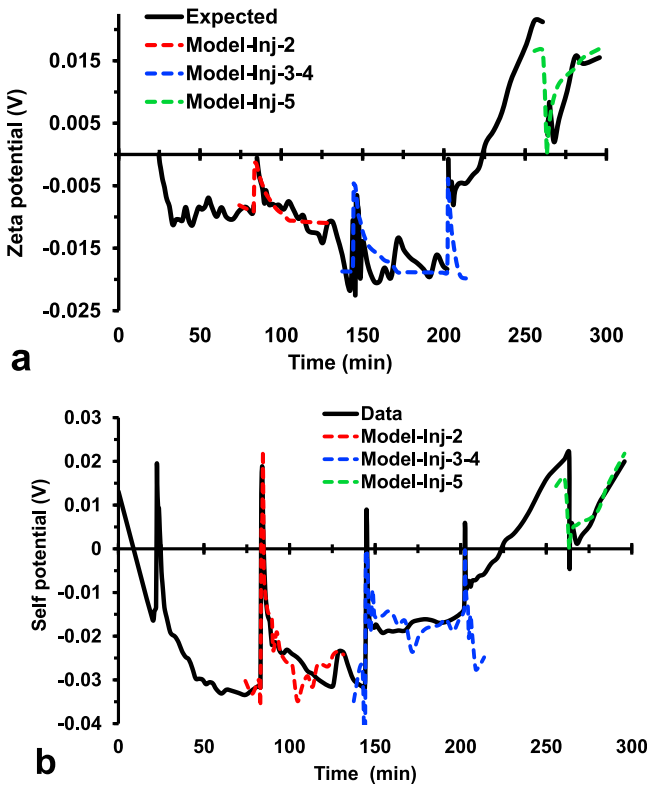

Figure 10. Model outputs for the injection experiment. (a) Time series of expected (ζ_{exp}) and modeled (ζ_{mod}) zeta potentials using, for consistency, the same final porosity (ϕ = 0.81) and initial grain volume ($v(0)$ = 0.015 mm^3) as in natural melt experiment. (b) Time series of measured and modeled SP data using the same parameters; the model curves were generated using the different slopes and intercepts characterizing the individual EC-ζ_{crrct} relationships (see Figure 7b).

natural melt experiment (minimum of $\sim 6 \times 10^{-6}$ S m^{-1}; see Figure 6b).

[32] The expected zeta potential (ζ_{exp}) is inferred to range between -2.3×10^{-2} V and $+2.1 \times 10^{-2}$ V in the injection experiment, and is characterized by a temporally evolving pattern that is much more complex (Figure 10a) than that of in ζ_{exp} the natural melt experiment (Figure 6a). As expected (above), we found that α and β varied systematically over time, having values of $\alpha = +1.6 \times 10^{-2}$ V and $\beta = +5.0 \times 10^{-2}$ V for injection 2, $\alpha = +2.2 \times 10^{-2}$ V and $\beta = +6.5 \times 10^{-2}$ V for injections 3 to 4, and $\alpha = -2.2 \times 10^{-2}$ V and $\beta = -6.9 \times 10^{-2}$ V for injection 5 (Figure 7b). Allowing for statistical variability, the values of α and β are thus very similar for injections 2, 3 and 4. However, the sign of the ζ_{crrct} − EC relationship is reversed for these three injections as compared with injection 5 and the natural melt experiment. The slope ($\alpha = -2.2 \times 10^{-2}$ V) of the relationship between the corrected zeta potential (ζ_{crrct}) and meltwater EC for injection 5 is similar to that characterizing the natural melt experiment ($\alpha = -4.4 \times 10^{-2}$ V). The ζ_{crrct} − EC relationships for injections 2 to 5 are relatively offset toward larger values of EC as compared with the natural melt experiment (Figure 7b). Allowing for the inferred variability in α and β, our model is able to produce an excellent fit between the measured and modeled streaming potential data for injections 2 to 5 (Figure 10b).

6. Discussion

6.1. Key Assumptions

[33] We have demonstrated that the integration of pertinent snow hydrological theory with that of streaming potential generation under unsaturated conditions is well suited to describing SP signals observed in melting snow columns. Our repeat laboratory experiments confirmed that such signals represent a robust signature of snow-internal hydrological and metamorphic processes. We were able to successfully integrate into our new mathematical framework a number of previously reported empirical relationships between meltwater EC and pH, melt fraction, zeta potential and permeability, grain diameter and grain growth. However, the lack of direct measurements of temporally evolving textural, hydraulic and water quality properties is an acknowledged weakness of our study that must be addressed by future work. We have assumed that electro-osmotic, thermal or electrochemical contributions to the measured SP signals are at all times negligible compared to the streaming potential contribution. These assumptions appear justified in that we were able to generate very close matches between modeled and measured SP data in both the natural melt and the injection experiments using our new semicoupled mathematical framework, implying that any electro-osmotic, thermal or electrochemical contributions are small or very transient. Nonetheless, to confirm this indirect inference, we recommend that future work should include measurements of snow column temperature over time and consider potential effects on measured SP signals. The fully melted snow samples used in our injection experiments contained all chemical species originally present within the snowpack. In contrast, the melting snow column was subject to preferential elution of ions, causing relatively reduced EC and elevated pH. Conceptually we would therefore expect that postinjection mixing of the two types of fluid should at least temporarily generate noticeable electrochemical potentials [*Kulessa et al.*, 2003a]. Although we did not find diagnostic evidence for the presence of such electrochemical potentials in our coupled modeling and experimental approach, we recommend that future work should assess the validity of this indirect inference.

6.2. Textural and Hydraulic Properties

[34] Connected porosity is the most fundamental parameter controlling our model predictions, and could in practice be estimated from joint considerations of snow mass changes and meltwater throughput over time. In the absence of suitable measurements of such changes in the present study, we assumed that connected porosities increased linearly between a known 'proxy' starting value, and a range of assumed final values that defined uncertainty. The second key unknown parameter in our model, the initial grain volume, was constrained based on values reported previously in the literature and identification of a reasonable range of uncertainty. We found that our new mathematical framework is only weakly sensitive to the combined uncertainty in final snow porosities and initial grain volumes, and that a close match between measured and modeled SP data could be obtained using similar values of final snow porosity ($\phi_{fin} \approx 0.81$) at fixed

initial grain volume ($v(0) = 0.015$ mm^3) in both the natural melt and injection experiments. These findings are encouraging in that they support the practical applicability of our new framework to in situ snow hydrological problems.

[35] In practice the compaction of wetting snowpacks is expected to reduce significantly snow porosities and permeabilities [*Williams et al.*, 2010]. In contrast, our snow column was small and would therefore have compacted little under its own weight. It would additionally have been supported by the walls of Perspex tube, further reducing compaction over time. This may provide a possible explanation for the relatively large inferred values of final porosities of $\phi_{fin} \approx 0.81$. Indeed, melting snowpacks readily produce preferential flow pathways [*Williams et al.*, 2010, and references therein], representing a "nonclassical" transport process [*Bolshov et al.*, 2010] that may well have affected our laboratory experiments. More specifically, our estimates of textural and hydraulic snow properties may thus represent effective averages over relatively porous and permeable preferential pathways that developed over time, within a snow matrix whose porosities and permeabilities are comparatively reduced. Since our model is based on the assumption of laminar flow through a single-permeability medium, it does not allow for turbulent effects on the streaming potential coupling coefficient [*Crespy et al.*, 2007]. In practice we would expect such effects to be most dominant during times of high meltwater flow rates, or where snow metamorphosis has caused significant changes to the snow matrix and produced large preferential flow pathways. Future work should therefore ascertain the potential impact of preferential flow pathways and turbulent effects on SP signatures of melting snowpacks.

[36] We followed *Albert and Krajeski* [1998] in assuming that irreducible water saturation was close to 0.03, recognizing at the same time that this parameter is poorly known. Specifically, the geometrical properties of the snow grains and those of the pore space, as well as the electrical properties of the ice-water interface evolve during the course of our experiments. It is therefore likely that irreducible water saturation also evolves over time, which has yet to be elucidated. The starting values of modeled permeabilities for both the natural melt (2.7×10^{-10} m^2) and injection (3.1×10^{-10} m^2) are consistent with those reported by *Colbeck and Anderson* [1982] for an in situ melting snow cover. Modeled increases in both the permeability (3.1×10^{-10} m^2 to 1.4×10^{-9} m^2) and grain diameter (0.15 to 0.88 mm) in the injection experiment are considerably less pronounced than those in the natural melt experiment ($\sim 2.7 \times 10^{-10}$ m^2 to $\sim 5.8 \times 10^{-8}$ m^2, and $\sim$0.35 mm to $\sim$1.66 mm respectively). This is likely a consequence of larger meltwater saturation at most times in the natural melt experiment than in the injection experiment (compare Figures 6a and 9a), since the growth of the snow grains and thus the permeability scales directly with water saturation (equations (13)–(15)). We caution, however, that the empirical grain-growth relationship of *Brun* [1989], which we parameterized in our model (equation (14)), has so far only been tested for fractional water contents (θ) of less than $\sim$0.1. Since this value was exceeded significantly during our experiments, we have implicitly assumed that this relationship also extrapolates to much larger values of θ, which remains to be ascertained by future work.

6.3. Water Quality Properties

[37] Here we adopted snowmelt pH values derived by *Darmody et al.* [2000] from snow patch samples at two different elevations in a valley close to our research station. The pH values we considered most applicable in our study were collected at lower elevation, and ranged from 5.6 to 6.5 with a mean of $\sim$6.0. The higher-elevation data yielded pH values between 5.9 and 6.6, and thus have a slightly higher average. *De Caritat et al.* [2005] published a comprehensive inventory of the chemical properties of Arctic snow. The three snow samples [*de Caritat et al.*, 2005, samples N39, S68, and F21/22] collected with a few hundred kilometers of our site [*de Caritat et al.*, 2005, samples N39, S68, and F21/22] had a "fully melted" pH of 4.9 ± 0.2. Thus the pH values of *de Caritat et al.* [2005] are noticeably smaller than those reported by *Darmody et al.* [2000], revealing considerable uncertainty. We collected our samples well away from the Abisko research station in areas where the snowpack was visually undisturbed. Notwithstanding, the samples may have been affected by anthropogenic pollution from it or nearby residential areas, and specifically may have been affected by the settling of CO_2 and other atmospheric pollutants on the snow surface. Significantly however, our model is insensitive to variations in the absolute values of pH as long as (i) the relative temporal evolution of pH remains the same, as controlled by the fixed coefficients in third-order polynomial dependency of pH on melt fraction (Figure 2); and (ii) the difference between the pH of the fully melted sample (pH_{mean}) and the pH at the point of zero charge ($pH_w(pzc)$) remains constant (equations (18) and (33)). Thus we strongly recommend that future work should consider measuring the pH of each sequential meltwater sample to confirm the validity of the coefficients used here.

[38] We were able to use post-experiment, fully melted EC measurements to constrain our calculations of EC evolution over time. EC measurements of the two fully melted snow samples reported here yielded values of 1.2×10^{-3} S m^{-1} and 7.0×10^{-3} S m^{-1} S m^{-1}, with a third sample of 7.4×10^{-3} S m^{-1}. The EC values of the samples reported by *Darmody et al.* [2000] ranged between 0.2×10^{-3} S m^{-1} and 0.5×10^{-3} S m^{-1}, while those of *de Caritat et al.* [2005] had values of 0.6×10^{-3} S m^{-1}, 0.7×10^{-3} S m^{-1} and 3.4×10^{-3} S m^{-1}. Thus, EC variations of at least an order of magnitude can be expected, even where samples are collected within a few tens of meters of each other (as was the case in our study), introducing considerable uncertainty. The temporal evolution of EC is principally controlled by the initial value of EC (σ_0) and the parameter m_0 that controls the exponential rate of EC change (equation (16)). Our model is strongly sensitive to both parameters. While we were able to calculate σ_0 from the measured EC values of our fully melted snow samples (equation (17)), we adopted the value of $m_0 \approx 0.08$ from previous work. Unsurprisingly we find that even a small departure from $m_0 = 0.08$ has a significant deteriorating effect on our model fits, confirming that 0.08 may well be a generally acceptable and robust value for m_0. Nonetheless, future work should confirm the exact values of m_0 and σ_0.

6.4. Zeta Potential

[39] One of the most fascinating, though least understood, parameters in our model is the zeta potential of the ice-water

interface. Previous work [*Drzymala et al.*, 1999; *Kallay et al.*, 2003] had ascertained that the zeta potential of this interface reverses sign from ~+0.01 V to ~−0.02 V, as the equilibrium pH of sodium chloride solutions increases from less than 3 to greater than 8 (Figure 1). We therefore expected that the electrochemical properties of the electrical double layer at this interface, and thus also the magnitude and potentially the sign of the zeta potential, will change over time as the snow samples are affected by melt, recrystallization and the preferential elution of ions. In the absence of suitable measurements in the present study, we adopted *Kallay et al.*'s [2003] value of $pH_w(pzc) = 3.6$ (Figure 1) for our modeling experiments. We recognize, however, that $pH_w(pzc)$ is strongly sensitive to the concentrations of anions like Cl^- (section 2.4), and may vary considerably along with ionic strength and content, as discussed further below. The zeta potential was modeled to increase from -8.7×10^{-2} V to $+1.5 \times 10^{-2}$ V in the natural melt experiment (Figure 7a), and inferred to range between -2.3×10^{-2} V and $+2.1 \times 10^{-2}$ V in the injection experiment (Figure 10a). Encouragingly, both zeta potential ranges broadly agree with those expected from previous work (i.e., a few tens of millivolts; see Figure 1) [*Drzymala et al.*, 1999; *Kallay et al.*, 2003], although meltwater EC was strongly variable throughout our experiments (Figures 6b and 10b).

[40] The most dramatic increases in meltwater pH occur within the first hour of the experiment (Figures 6b and 9b). In accordance with previous work (Figure 1) we would thus expect to infer a strong decrease in the zeta potential during this time period. Although we were not able to model the first ~50 min of the experiment owing to the lack of meltwater discharge from the snow column, the expected zeta potential (ζ_{exp}) is indeed inferred to decrease rapidly between ~50 and 60 min into the natural melt experiment (Figure 7a). Although meltwater pH remains approximately constant at ~6.3 at later times (i.e., greater than ~100 min; see Figure 6b) in that experiment, a steady increase in the zeta potential by several tens of millivolts (Figure 7a), and a steady decrease in meltwater EC by several orders of magnitude (Figure 6b), are modeled for the same time span. In the case of the natural melt experiment, we can thus infer a dominant influence of changes in meltwater pH on the zeta potential at early times (i.e., before ~60 min), and of changes in meltwater EC on it at later times (i.e., >~60 min). Owing to the five sequential injections of fully melted snow samples, commencing at ~22.5 min into the experiment (Figure 4), and the associated complexity of the pH and EC evolution within the column (Figure 9b), the relative influences of pH and EC on the inferred zeta potential (Figure 10a) are less obvious in the case of the injection experiment.

[41] The time period before ~50 min in the natural melt experiment was characterized by an initial rapid decrease and change of sign of the measured SP signals, reaching a temporary minimum of ~−0.03 V at ~28 min (Figure 4a). That minimum is followed by a transient increase in measured SP signals that reached a weakly positive peak (~+0.0025 V) at ~40 min (Figure 4a). This pattern was repeated in all of our experiments, although unfortunately we not have appropriate measurements of snow or meltwater properties that would allow us to infer the hydrological or metamorphic processes that control this early time SP evolution. In this context we note however that, using a point of zero charge ($pH_w(pzc)$) of 3.6, our model (red line in Figure 7a) was not able to reproduce the initial decrease in the expected zeta potential inferred for the 50–60 min time period, even if the porosity and the initial grain volume were varied relative to the respective best fit values of 0.81 and 0.015 mm^3 (Figure 5). If we speculate that $pH_w(pzc)$ has in fact a different value in our experiments, or indeed that it evolves over time along with the electrical double layer, then we are able to approximate that initial decrease, as illustrated by the modeled blue line in Figure 7a. That line was obtained, purely for illustrative purposes, by keeping porosity and the initial grain volume constant at the respective best fit values of 0.81 and 0.015 mm^3, and by setting $pH_w(pzc)$ equal to 4.9 which corresponds to the modeled value of pH at the transient SP minimum of ~28 min (Figure 4a). More (or less) pronounced initial zeta potential decreases are obtained when $pH_w(pzc)$ is set to larger (or smaller) values than 4.9. Future work should thus consider measurement of the point of zero charge in melting snowpacks, together with quantification of its potential evolution over time.

[42] The magnitudes of the expected (ζ_{exp}), corrected (ζ_{crrct}) and modeled (ζ_{mod}) zeta potentials are strongly sensitive to the values of α and β that control the linear regression of ζ_{crrct} and the decadal logarithm of meltwater EC (i.e., $\log(\sigma_w)$ or $\log(\sigma_{mix})$, equations (18) and (33)). Allowing for statistical variability, the values of α inferred for the natural melt (-4.4×10^{-2} V) experiment as well as for injection 5 (-2.2×10^{-2} V), are not entirely dissimilar with respect to each other and to the "typical" value of ~0.02 V reported previously for silica by *Pride and Morgan* [1991], *Revil et al.* [1999b], and *Guichet et al.* [2003]. Indeed, the governing equations (18) and (33) were adopted from *Revil et al.* [1999b], who inferred them for silica-dominated porous media, albeit bearing fluids of higher ionic strengths than those inferred here. The consistency of our findings with previous work in particular, and the successful application of these established relationships to snow hydrological problems more generally, thus provides initial evidence that the ice-water interface has similar electrochemical properties to the silica-water interface.

[43] It is unsurprising that the inferred values of α were similar for the natural melt experiment and for injection 5, since the breakthrough of the injected snowmelt during injection 5 was extremely rapid (Figure 4a). The vast majority of the meltwaters within the column immediately following that injection were therefore derived from natural melt within it, rather than from injected waters, thus providing a water quality environment that was very similar to that of the natural melt experiment. In contrast, injected melt breakthrough was considerably slower following injections 2 to 4, and thus promoted temporally persistent mixing of injected and natural meltwaters (section 5.4). This would have provided a water quality environment that was substantially different to either the natural melt ($\alpha = -4.4 \times 10^{-2}$ V) experiment or to injection 5 ($\alpha = -2.2 \times 10^{-2}$ V), and one that was characterized by a substantially different values of α with an opposite sign ($\alpha = +1.6 \times 10^{-2}$ V for injection 2 and $\alpha = +2.2 \times 10^{-2}$ V for injections 3 to 4; see Figure 7b). We suspect that at least some of this inferred variability is due to a point of zero charge that is temporally evolving, along with the concentration of anions like Cl^- (above). Unfortunately we do not have suitable measurements of key water quality parameters to consolidate this

speculation. It is therefore imperative that future work should consider temporally high resolved measurements of meltwater pH, EC and where possible also ionic content.

7. Conclusions and Recommendations for Future Work

[44] We have developed a new theory and semicoupled hydroelectric model that is capable of simulating SP signals generated in unsaturated melting snowpacks, ignoring electro-osmotic effects or the presence of natural electrical potentials other than streaming potentials. It remains speculative whether electro-osmotic effects are noticeable at certain times, such as for example at initial melt onset in snowpacks, or more generally during times of low meltwater generation and flow. Conceptually we would also expect that meltwater pulses flushing through melting snowpacks should generate noticeable electrochemical potentials as several waters with different ionic strengths or contents mix. Although we did not find conclusive evidence for the presence of either electro-osmotic or electrochemical effects, we recommend that future work should assess the validity of these indirect inferences.

[45] We have also demonstrated the application of the new model to laboratory SP measurements of natural snowmelt and meltwater pulses, simulated using injection experiments. Aside from meltwater flux, SP signals are most sensitive to initial grain volume, the temporal evolutions of connected porosity and meltwater quality parameters such as EC and pH. While the temporal evolution of total or connected porosity of melting snowpacks is generally poorly documented in the literature, and initial grain volume can readily differ by up to an order of magnitude depending on the type and age of the snowpack [*Jordan et al.*, 2008], melting snow is subject to well-known elution sequences of ions and associated temporal evolutions of meltwater EC and pH. We were able to simulate successfully observed SP signals of melting snow by parameterizing existing empirical relationships between fractional melt, EC, pH and the zeta potential in our new hydroelectric model. We further assumed that (i) snow porosity increases linearly over time, as the snow grains metamorphose according to a previously published empirical relationship between fractional melt and grain growth [*Brun*, 1989]; (ii) *Shimizu*'s [1970] empirically determined of dependency of snow permeability on density and grain size applies, ignoring any potential effects of grain shape or anisotropy on permeability [*Luciano and Albert*, 2002; *Domine et al.*, 2008]; and (iii) the empirical relationships of *Brun* [1989] and *Shimizu* [1970] apply although the experimental procedures, timescales and cold room conditions under which they were derived were dissimilar from the present laboratory conditions.

[46] Unknown final porosities and initial grain volumes were determined by least squares minimization of observed and modeled SP data. We therefore consider it imperative that future research into SP methods for snow hydrology should include more exhaustive measurements of temporally evolving textural, hydraulic and water quality properties. Much progress has recently been made in the development of technologies for the measurement of the spatial and temporal evolution of the specific surface area of in situ snowpacks [*Domine et al.*, 2009, and references therein]. It would thus appear to be particularly pertinent and promising to integrate specific surface area, as a fundamental textural parameter of snow, into the next generation hydroelectric model of SP signals associated with unsaturated meltwater flow in snow. Highly resolved temporal measurements of meltwater EC and pH would allow the coefficients in equations (17) and (19), governing the temporal evolutions of EC (e.g., m_0) and pH respectively, to be estimated. If the bulk electrical conductivity (σ) of the evolving snowpack was measured along with EC (σ_w), e.g., using spatially and temporally coincident electrical resistivity tomography (ERT) techniques [*Kulessa et al.*, 2006], then temporal changes in the snow's formation factor could serve as a proxy for temporal changes in water saturation (equation (8)).

[47] Previous experimental work had ascertained that the sign of the zeta potential of the ice-water interface is reversible depending on fluid pH (Figure 1) [*Drzymala et al.*, 1999], and electrical double-layer models of the ice-water interface have been proposed [*Kallay et al.*, 2003; *Kolunin and Kolunin*, 2009]. Existing experimental and theoretical work is, however, still very sparse and our understanding of the electrical double layer of the ice-water interface therefore incomplete. More laboratory data revealing the dependence of the zeta potential on fluid type, pH and ionic strength and contents are required, and could lead to an updated electrical double-layer model of this interface that is more thoroughly tested. As discussed in section 6.4, particular attention should also be paid to the measurement of the point of zero charge of the zeta potential, and its potential evolution over time.

[48] We caution further that several fundamental properties and processes relevant to SP investigations of snow hydrological problems are sparsely investigated so far. Particularly significantly, these include (i) the temporal variability of snowpack temperature, (ii) the relationship between fractional melt and snow grain growth, (iii) the irreducible water saturation (equation (3)) and the effective saturation exponent (equation (5)) and their potential variability in space and time, (iv) the development and persistence of preferential flow pathways, and (v) the spatial and temporal evolution of snowpack compaction and the associated effects on its textural and hydraulic properties. As discussed above, in the absence of direct evidence we have assumed the following:

[49] 1. The temperature of our snow column remained constant close to 0°C, although we recognize that even small temperature variations could affect meltwater EC in particular.

[50] 2. The compaction of the snow in our laboratory column was negligible.

[51] 3. Following *Albert and Krajeski* [1998], irreducible water saturation and the effective saturation exponent were constant and equal to 0.03 and 3.3, respectively, although we recognize that the effective saturation exponent may potentially depend on grain size and thus vary between ~2.2 and 4.6 [*Denothe et al.*, 1979].

[52] 4. The fractional melt–grain growth relationship of *Brun* [1989] applies, although effective saturations inferred in this study (up to ~0.4) considerably exceeded those for which that relationship was tested (up to ~0.1).

[53] 5. Any preferential flow pathways, which we recognize were likely to develop [*Williams et al.*, 2010, and references therein], could be represented by equivalent volume-averaged properties.

[54] All of these assumptions should be confirmed by dedicated direct measurements in future work.

[55] In practice, we envisage that SP measurements could serve as nonintrusive sensors of meltwater flux, if sufficient EC and pH data were available to constrain the model predictions or can be derived independently (see below). At a minimum EC and pH should be measured in multiple locations at the start and end of the survey period. Where measurements of meltwater flux are available together with at least some EC and pH measurements for calibration, SP measurements could serve as a proxy for the evolution of meltwater chemistry (i.e., EC or pH). Indeed, where sufficient EC, pH and flux data are available, SP measurements could be inverted for the evolution of snow properties such as the connected porosity, permeability, grain size or effective saturation or storage. The instrumentation for in situ SP measurements is simple, requiring only a high-impedance voltmeter and two nonpolarizing electrodes in the simplest case, or the use of automated data loggers as demonstrated here. Future work should focus on the development of low-cost SP sensor arrays for longer-term in situ installation and monitoring. Such studies should also focus on the advancement of robust field strategies for the calibration of SP data in terms of flux, EC, pH or snow properties at key strategic locations, and the subsequent extrapolation of such properties over wider areas based, e.g., on 3-D SP inversion [*Jardani et al.*, 2006, 2007; *Minsley et al.*, 2007] or cross-correlation techniques [*Iuliano et al.*, 2002]. It is helpful in this context that the bulk electrical and hydrological properties of snow can often be expected to vary little over wider areas, relative to many other applications encountered in water resource studies. Often snow hydrological problems occur in mountainous or other remote areas, where electrical noise is relatively small and signal-to-noise ratio therefore high. Initial field tests have been promising [*Chandler et al.*, 2005; *Kulessa and Chandler*, 2008]. Future work will also need to develop a model of electrical resistivity and SP attributes that is fully integrated with reactive transport modeling in snow and ice.

[56] In summary, we believe that the SP technique has exciting and broad scope in snow hydrology, although dedicated future research must advance the current state of the science from theory, numerical modeling and laboratory testing through to field applications in commercial practice.

[57] **Acknowledgments.** The laboratory experiments reported here were funded by European Union ATANS grant FP6 506004. Many thanks for the help and support provided by staff at Abisko Naturvenskapliga Station in Sweden, and to Mark Williams for valuable advice on the temporal evolution of snow physical properties during melt. We would like to thank Niklas Linde and two anonymous reviewers for detailed and constructive reviews.

References

Albert, M., and G. Krajeski (1998), A fast, physically based point snowmelt model for use in distributed applications, *Hydrol. Processes*, *12*, 1809–1824, doi:10.1002/(SICI)1099-1085(199808/09)12:10/11<1809::AID-HYP696>3.0.CO;2-5.

Arnold, N., K. Richards, I. C. Willis, and M. Sharp (1998), Initial results from a distributed, physically based model of glacier hydrology, *Hydrol. Processes*, *12*, 191–219, doi:10.1002/(SICI)1099-1085(199802)12:2<191::AID-HYP571>3.0.CO;2-C.

Bolshov, L., P. Kondratenko, K. Pruess, and V. Semenov (2010), Nonclassical transport processes in geologic media: Review of field and laboratory observations and basic physical concepts, *Vadose Zone J.*, *7*, 1135–1144.

Brimblecombe, P., M. Tranter, S. Tsiouris, T. D. Davies, and C. E. Vincent (1986), The chemical evolution of snow and meltwater, *IAHS Publ.*, *155*, 283–295.

Brooks, R. H., and A. T. Corey (1964), *Hydraulic Properties of Porous Media*, 27 pp., Colo. State Univ., Ft. Collins.

Brun, E. (1989), Investigation on wet-snow metamorphism in respect of liquid-water content, *Ann. Glaciol.*, *13*, 22–26.

Caine, N. (1992), Modulation of the diurnal streamflow response by the seasonal snowcover of an alpine basin, *J. Hydrol.*, *137*, 245–260, doi:10.1016/0022-1694(92)90059-5.

Caine, N. (1995), Snowpack influences on geomorphic processes in Green Lakes Valley, Colorado Front Range, *Geogr. J.*, *161*, 55–68, doi:10.2307/3059928.

Campbell, F., P. Nienow, and R. Purves (2006), Role of the supraglacial snowpack in mediating meltwater delivery to the glacier system as inferred from dye tracer experiments, *Hydrol. Processes*, *20*, 969–985, doi:10.1002/hyp.6115.

Chandler, D., B. Kulessa, and S. Mackie (2005), Electrokinetic potentials associated with water flow through a snow pack, paper presented at Conference on Geophysics and Glacial Materials, Environ. and Indust. Geophys. Group, Geol. Soc., Northumbria Univ., Newcastle, U. K.

Cline, D. (1997), Snow surface energy exchanges and snowmelt at a continental, midlatitude Alpine site, *Water Resour. Res.*, *33*, 689–701, doi:10.1029/97WR00026.

Colbeck, S. C. (1972), A theory of water percolation in snow, *J. Glaciol.*, *11*, 369–385.

Colbeck, S. C., and E. A. Anderson (1982), The permeability of a melting snow cover, *Water Resour. Res.*, *18*, 904–908, doi:10.1029/WR018i004p00904.

Cragin, J. H., A. D. Hewitt, and S. C. Colbeck (1993), Elution of ions from melting snow: Chromatographic versus metamorphic mechanisms, *CRREL Rep., 93-8*, Cold Reg. Res. and Eng. Lab., Hanover, N. H.

Cragin, J. H., A. D. Hewitt, and S. C. Colbeck (1996), Grain-scale mechanisms influencing the elutions of ions from snow, *Atmos. Environ.*, *30*, 119–127, doi:10.1016/1352-2310(95)00232-N.

Crespy, A., A. Bolève, and A. Revil (2007), Influence of the Dukhin and Reynolds numbers on the apparent zeta potential of granular porous media, *J. Colloid Interface Sci.*, *305*, 188–194, doi:10.1016/j.jcis.2006.09.038.

Dai, Y. J., and Q. Zeng (1997), A land surface model (IAP94) for climate studies, part I: Formulation and validation in off-line experiments, *Adv. Atmos. Sci.*, *14*, 433–460, doi:10.1007/s00376-997-0063-4.

Darmody, R. G., C. E. Thorn, R. L. Harder, J. P. L. Schlyter, and J. C. Dixon (2000), Weathering implications of water chemistry in an arctic–alpine environment, northern Sweden, *Geomorphology*, *34*, 89–100, doi:10.1016/S0169-555X(00)00002-7.

Davis, R. E., C. E. Petersen, and R. C. Bales (1995), Ion flux through a shallow snowpack: Effects of initial conditions and melt sequences, *IAHS Publ.*, *228*, 115–126.

de Caritat, P., et al. (2005), Chemical composition of arctic snow: Concentration levels and regional distribution of major elements, *Sci. Total Environ.*, *336*, 183–199, doi:10.1016/j.scitotenv.2004.05.031.

Denothe, A., W. Seidenbusch, M. Blumthaler, P. Kirchlechner, W. Ambach, and S. C. Colbeck (1979), Study of water drainage from columns of snow, *CRREL Rep. 79-1*, Cold Reg. Res. and Eng. Lab., Hanover, N. H.

DeWalle, D. R., and A. Rango (2008), *Principles of Snow Hydrology*, Cambridge Univ. Press, Cambridge, U. K., doi:10.1017/CBO9780511535673.

Doherty, R., B. Kulessa, A. S. Ferguson, M. J. Larkin, L. A. Kulakov, and R. M. Kalin (2010), A microbial fuel cell in contaminated ground delineated by electrical self-potential and normalized induced polarization data, *J. Geophys. Res.*, *115*, G00G08, doi:10.1029/2009JG001131.

Domine, F., M. Albert, T. Huthwelker, H. W. Jacobi, A. A. Kokhanovsky, M. Lehning, G. Picard, and W. R. Simpson (2008), Snow physics as relevant to snow photochemistry, *Atmos. Chem. Phys.*, *8*, 171–208, doi:10.5194/acp-8-171-2008.

Domine, F., A.-S. Taillandier, A. Cabanes, T. A. Douglas, and M. Sturm (2009), Three examples where the specific surface area of snow increased over time, *Cryosphere*, *3*, 31–39, doi:10.5194/tc-3-31-2009.

Drzymala, J., Z. Sadowski, L. Holysz, and E. Chibowski (1999), Ice/water interface: Zeta potential, point of zero charge, and hydrophobicity, *J. Colloid Interface Sci.*, *220*, 229–234, doi:10.1006/jcis.1999.6528.

Dutra, E., G. Balsamo, P. Viterbo, P. Miranda, A. Beljaars, C. Schaer, and K. Elder (2010), An improved snow scheme for the ECMWF land surface model: Description and offline validation, *J. Hydrometeorol.*, *11*, 899–916, doi:10.1175/2010JHM1249.1.

Essery, R., E. Martin, H. Douville, A. Fernandez, and E. Brun (1999), A comparison of four snow models with observations from an alpine site, *Clim. Dyn.*, *15*, 583–593, doi:10.1007/s003820050302.

Fierz, C., R. L. Armstrong, Y. Durand, P. Etchevers, E. Greene, D. M. McClung, K. Nishimura, P. K. Satyawali, and S. A. Sokratov (2009), *The International Classification for Seasonal Snow on the Ground, IHP-VII Tech. Doc. Hydrol. 83, IACS Contrib. 1*, United Nations Educ., Sci. and Cult. Org., Paris.

Fountain, A. G., and J. S. Walder (1998), Water flow through temperate glaciers, *Rev. Geophys.*, *36*, 299–328, doi:10.1029/97RG03579.

French, H. K., A. Binley, I. Kharkhordin, B. Kulessa, and S. S. Krylov (2006), Permafrost and snowmelt, in *Applied Hydrogeophysics*, edited by H. Vereecken et al., pp. 195–232, Springer, New York.

Guichet, X., L. Jouniaux, and J.-P. Pozzi (2003), Streaming potential of a sand column in partial saturation conditions, *J. Geophys. Res.*, *108*(B3), 2141, doi:10.1029/2001JB001517.

Gustafsson, D., P. Waldner, and M. Staehli (2004), Factors governing the formation and persistence of layers in a subalpine snowpack, *Hydrol. Processes*, *18*, 1165–1183, doi:10.1002/hyp.1398.

Harrington, R. F., R. C. Bales, and P. Wagnon (1996), Variability of meltwater and solute fluxes from homogeneous melting snow at the laboratory scale, *Hydrol. Processes*, *10*, 945–953, doi:10.1002/(SICI)1099-1085(199607)10:7<945::AID-HYP349>3.0.CO;2-S.

Herrmann, R., and J. Kranz (1995), Release of major ions and hydrogen peroxide from homogeneous, melting snow, *Nord. Hydrol.*, *26*, 359–368.

Iuliano, T., P. Mauriello, and D. Patella (2002), Looking inside Mount Vesuvius by potential fields integrated probability tomographies, *J. Volcanol. Geotherm. Res.*, *113*, 363–378, doi:10.1016/S0377-0273(01)00271-2.

Jardani, A., A. Revil, and J. P. Dupont (2006), Self-potential tomography applied to the determination of cavities, *Geophys. Res. Lett.*, *33*, L13401, doi:10.1029/2006GL026028.

Jardani, A., A. Revil, A. Bolève, J. P. Dupont, W. Barrash, and B. Malama (2007), Tomography of the Darcy velocity from self-potential measurements, *Geophys. Res. Lett.*, *34*, L24403, doi:10.1029/2007GL031907.

Jordan, R. (1991), *A One-Dimensional Temperature Model for Snow Cover, CRREL Spec. Rep., 91-16*, 49 pp., Cold Reg. Res. and Eng. Lab., Hanover, N. H.

Jordan, R., J. P. Hardy, F. E. Perron Jr., and D. J. Fisk (1999), Air permeability and capillary rise as measures of the pore structure of snow: An experimental and theoretical study, *Hydrol. Processes*, *13*, 1733–1753, doi:10.1002/(SICI)1099-1085(199909)13:12/13<1733::AID-HYP863>3.0.CO;2-2.

Jordan, R., M. Albert, and E. Brun (2008), Physical processes within the snow-cover and their parameterization, in *Snow and Climate: Physical Processes, Surface Energy Exchange and Modeling*, edited by R. Armstrong and E. Brun, pp. 12–69, Cambridge Univ. Press, Cambridge U. K.

Jougnot, D., N. Linde, A. Revil, and C. Doussan (2012), Derivation of soil-specific streaming potential electrical parameters from hydrodynamic characteristics of partially saturated soils, *Vadose Zone J.*, *11*(1), doi:10.2136/vzj2011.0086.

Kallay, N., A. Cop, E. Chibowski, and L. Holysz (2003), Reversible charging of the ice-water interface, II: Estimation of the equilibrium parameters, *J. Colloid Interface Sci.*, *259*, 89–96, doi:10.1016/S0021-9797(02)00179-0.

Kohler, J., O. Brandt, M. Johansson, and T. Callaghan (2006), A long-term Arctic snow depth record from Abisko, northern Sweden, 1913–2004, *Polar Res.*, *25*, 91–113, doi:10.1111/j.1751-8369.2006.tb00026.x.

Kolunin, V. S., and A. V. Kolunin (2009), Electrical cross effects in porous media with ice inclusions, part II: Double electrical layer mechanism, *Int. J. Heat Mass Transfer*, *52*, 5577–5584, doi:10.1016/j.ijheatmasstransfer.2009.06.022.

Kulessa, B. (2007), A critical review of the low-frequency electrical properties of ice sheets and glaciers, *J. Environ. Eng. Geophys.*, *12*, 23–36, doi:10.2113/JEEG12.1.23.

Kulessa, B., and D. Chandler (2008), Mapping and monitoring the spatio-temporal evolution of water flow patterns in snow using the electrical self potential (SP) method: A feasibility study, paper presented at Joint Assembly, Eur. Geosci. Union, Vienna.

Kulessa, B., B. Hubbard, and G. Brown (2003a), Cross-coupled flow modeling of coincident streaming and electrochemical potentials, and application to subglacial self-potential (SP) data, *J. Geophys. Res.*, *108*(B8), 2381, doi:10.1029/2001JB001167.

Kulessa, B., B. Hubbard, G. Brown, and J. Becker (2003b), Earth tide forcing of glacier drainage, *Geophys. Res. Lett.*, *30*(1), 1011, doi:10.1029/2002GL015303.

Kulessa, B., B. Hubbard, and G. Brown (2006), Time-lapse imaging of subglacial drainage conditions using 3-D inversion of subglacial electrical resistivity data, *J. Glaciol.*, *52*, 49–57, doi:10.3189/172756506781828854.

Leroy, P., and A. Revil (2009), Spectral induced polarization of clays and clay rocks, *J. Geophys. Res.*, *114*, B10202, doi:10.1029/2008JB006114.

Leroy, P., A. Revil, A. Kemna, P. Cosenza, and A. Ghorbani (2008), Spectral induced polarization of water-saturated packs of glass beads, *J. Colloid Interface Sci.*, *321*, 103–117, doi:10.1016/j.jcis.2007.12.031.

Linde, N., D. Jougnot, A. Revil, S. K. Matthäi, T. Arora, D. Renard, and C. Doussan (2007), Streaming current generation in two-phase flow conditions, *Geophys. Res. Lett.*, *34*, L03306, doi:10.1029/2006GL028878.

Luciano, G. L., and M. R. Albert (2002), Bi-directional permeability measurements of polar firn, *Ann. Glaciol.*, *35*, 63–66, doi:10.3189/172756402781817095.

Minsley, B. J., J. Sogade, and F. D. Morgan (2007), Three-dimensional source inversion of self-potential data, *J. Geophys. Res.*, *112*, B02202, doi:10.1029/2006JB004262.

Mitterer, C., H. Hirashima, and J. Schweizer (2011), Wet-snow instabilities: Comparison of measured and modelled liquid water content and snow stratigraphy, *Ann. Glaciol.*, *52*, 201–208, doi:10.3189/172756411797252077.

Mualem, Y. (1986), Hydraulic conductivity of unsaturated soils: Prediction and formulas, in *Methods of Soils Analysis: Part I. Physical and Mineralogical Methods*, 2nd ed., edited by A. Klute, pp. 799–823, Am. Soc. of Agron., Madison, Wisc.

Nolin, A. W. (2010), Recent advances in remote sensing of seasonal snow, *J. Glaciol.*, *56*, 1141–1150, doi:10.3189/002214311796406077.

Petiau, G. (2000), Second generation of lead-lead chloride electrodes for geophysical applications, *Pure Appl. Geophys.*, *157*, 357–382, doi:10.1007/s000240050004.

Pride, S., and F. D. Morgan (1991), Electrokinetic dissipation induced by seismic waves, *Geophysics*, *56*, 914–925.

Revil, A., and A. Cerepi (2004), Streaming potentials in two-phase flow conditions, *Geophys. Res. Lett.*, *31*, L11605, doi:10.1029/2004GL020140.

Revil, A., and N. Linde (2006), Chemico-electromechanical coupling in microporous media, *J. Colloid Interface Sci.*, *302*, 682–694, doi:10.1016/j.jcis.2006.06.051.

Revil, A., P. A. Pezard, and P. W. J. Glover (1999a), Streaming potential in porous media, I: Theory of the zeta-potential, *J. Geophys. Res.*, *104*, 20,021–20,031, doi:10.1029/1999JB900089.

Revil, A., H. Schwaeger, L. M. Cathles, and P. Manhardt (1999b), Streaming potential in porous media. II: Theory and application to geothermal systems, *J. Geophys. Res.*, *104*, 20,033–20,048, doi:10.1029/1999JB900090.

Revil, A., G. Saracco, and P. Labazuy (2003), The volcano-electric effect, *J. Geophys. Res.*, *108*(B5), 2251, doi:10.1029/2002JB001835.

Revil, A., K. Titov, C. Doussan, and V. Lapenna (2006). Applications of the self-potential method to hydrological problems, in *Applied Hydrogeophysics*, edited by H. Vereecken et al., pp. 255–292, Springer, New York.

Revil, A., N. Linde, A. Cerepi, D. Jougnot, S. Matthäi, and S. Finsterle (2007), Electrokinetic coupling in unsaturated porous media, *J. Colloid Interface Sci.*, *313*, 315–327, doi:10.1016/j.jcis.2007.03.037.

Revil, A., C. A. Mendoça, E. A. Atekwana, B. Kulessa, S. S. Hubbard, and K. Bohlen (2010), Understanding biogeobatteries: Where geophysics meets microbiology, *J. Geophys. Res.*, *115*, G00G02, doi:10.1029/2009JG001065.

Richards, L. A. (1931), Capillary conduction of liquids through porous media, *Physics*, *1*, 318–333, doi:10.1063/1.1745010.

Richter-Menge, J. A., S. C. Colbeck, and K. C. Jezek (1991), Recent progress in snow and ice research, *Rev. Geophys.*, *29*, supplement, 218–226.

Scambos, T. A., C. Hulbe, M. Fahnestock, and J. Bohlander (2000), The link between climate warming and break-up of ice shelves in the Antarctic Peninsula, *J. Glaciol.*, *46*, 516–530, doi:10.3189/172756500781833043.

Schöndorf, T., and R. Herrmann (1987), Transport and chemodynamics of organic micropollutants and ions during snowmelt, *Nord. Hydrol.*, *18*, 259–278.

Schwander, J., J. M. Barnola, C. Andrii, M. Leuenberger, A. Ludin, D. Raynaud, and B. Stauffer (1993), The age of the air in the firn and the ice at Summit, Greenland, *J. Geophys. Res.*, *98*, 2831–2838, doi:10.1029/92JD02383.

Shimizu, H. (1970), Air permeability of deposited snow, *Contrib. Inst. Low Temp. Sci. Ser. A.*, *22*, 1–32.

Sill, W. R. (1983), Self-potential modeling from primary flows, *Geophysics*, *48*, 76–86.

Staehli, M., M. Stacheder, D. Gustafsson, S. Schlaeger, M. Schneebeli, and A. Brandelik (2004), A new in situ sensor for large-scale snow-cover monitoring, *Ann. Glaciol.*, *38*, 273–278, doi:10.3189/172756404781814933.

Sturm, S., J. Holmgren, and G. E. Liston (1995), A seasonal snow cover classification system for local to global applications, *J. Clim.*, *8*, 1261–1283, doi:10.1175/1520-0442(1995)008<1261:ASSCCS>2.0.CO;2.

van Genuchten, M. T. (1980), A closed-form equation for predicting the hydraulic conductivity of unsaturated soils, *Soil Sci. Soc. Am. J.*, *44*, 892–898, doi:10.2136/sssaj1980.03615995004400050002x.

Wang, M., and A. Revil (2010), Electrochemical charge of silica surface at high ionic strength in narrow channels, *J. Colloid Interface Sci.*, *343*, 381–386, doi:10.1016/j.jcis.2009.11.039.

Williams, M. W., D. Cline, M. Hartmann, and T. Bardsley (1999), Data for snowmelt model development, calibration, and verification at an alpine site, Colorado Front Range, *Water Resour. Res.*, *35*, 3205–3209, doi:10.1029/1999WR900088.

Williams, M. W., C. Seibold, and K. Chowanski (2009), Storage and release of solutes from a subalpine seasonal snowpack: Soil and stream water response, Niwot Ridge, Colorado, *Biogeochemistry*, *95*, 77–94, doi:10.1007/s10533-009-9288-x.

Williams, M. W., T. A. Erickson, and J. L. Petrzelka (2010), Visualizing meltwater flow through snow at the centimetre-to-metre scale using a snow guillotine, *Hydrol. Processes*, *24*, 2098–2110.

Yamaguchi, S., T. Katsushima, A. Sato, and T. Kumakura (2010), Water retention curve of snow with different grain sizes, *Cold Reg. Sci. Technol.*, *64*, 87–93, doi:10.1016/j.coldregions.2010.05.008.

Zwally, H. J., K. Larson, W. Abdalati, J. Saba, T. Herring, and K. Steffen (2002), Surface melt-induced acceleration of Greenland ice-sheet flow, *Science*, *297*, 218–222, doi:10.1126/science.1072708.